University of Nevada, Reno

Light-activated materials for singlet oxygen generation and the degradation of pollutants

A thesis submitted in partial fulfillment of the requirements

for the degree of Master of Science in

Chemistry

by

Dominion R. Fredericks

Dr. Ana de Bettencourt-Dias/Thesis Advisor

December 2021

THE GRADUATE SCHOOL

We recommend that the thesis
prepared under our supervision by

Dominion R. Fredericks

entitled

Light-activated materials for singlet oxygen generation and the degradation of pollutants

be accepted in partial fulfillment of the
requirements for the degree of

Master of Science

Dr. Ana de Bettencourt- Dias
Advisor

Dr. Matthew J. Tucker
Committee Member

Dr. Yu (Frank) Yang
Graduate School Representative

David W. Zeh, Ph.D., Dean
Graduate School

December, 2021

Abstract

The research presented in this thesis focuses on light-activated materials that may enhance the treatment of wastewater and further the understanding of wastewater treatment (WWT) technologies. Wastewater disinfection technologies and processes are categorized and discussed by groups, namely conventional, alternatives, and emerging treatments. The pros and cons of all technologies addressed herein will be highlighted, emphasizing their application in WWT and their respective impact on the environment. Specifically, technologies that use advanced oxidative processes (AOPs) have been shown as a promising technology in the disinfection process in WWT and were the motivation behind this research.

AOPs, which involve the generation of reactive oxygen species (ROS), are highly potent oxidizing processes and have emerged as an essential class of technologies to accelerate the non-selective oxidation resulting in the inactivation of a wide range of organic pollutants found in wastewater. This thesis will discuss the various types of ROS, materials that generate ROS, and the ROS potential in industrial wastewater treatment.

New materials that generate ROS have been incorporated within polymers and have been shown to degrade a model pharmaceutical, namely propranolol, along with several semi-volatile and volatile organic pollutants. Specifically, UV- and visible light-activated membranes were synthesized by the simple method of doping a photosensitizer (PS) into a polyurethane substrate, ClearFlex 50 (CF50). Upon irradiation, these doped membranes generate the ROS singlet oxygen (SO), and through spectrofluorometric and chromatographic measurements, it was determined that propranolol and several pollutants were degraded. This work demonstrates that practical light-activated PS-doped membranes can be used to degrade several pollutants found in wastewater. Furthermore, preliminary studies of PSs that have potential to form metal organic-frameworks were performed and have shown

to absorb visible light and generate SO. These results are important for advancing light-activated materials that generate ROS with application in disinfection for WWTs.

Acknowledgments

This research was funded by the National science foundation. I also acknowledge the Shared Instrumentation Laboratory in the Department of Chemistry at UNR and the help of its staff, Dr. Stephen Spain and Dr. Nina Ruprecht. SEM-EDX analysis was performed in the Mackay Microbeam Laboratory at UNR, and I thank Dr. Joel DesOrmeau for his kind assistance. I want to thank Jake Holland in the machine shop for custom budling many items needed to conduct my research. I am beyond grateful for extremely helpful lab mates, Dr. Josi Sobrinho and Justin Nahavandi, your dedication to making me a better chemist and human will never be forgotten. Finally, of course, this experience at UNR would not be possible if it wasn't for my advisor, Dr. Ana de Bettencourt Dias; you have taught me so much over the years. You have a strive for excellence that is truly inspiring, and your dedication to the lab is everything a graduate student could ask for. Thank you for never settling for mediocracy.

Contents

List of Schemes

List of Figures

List of Tables

Chapter 1 – Introduction

1.1. Background

Improper management and technologies have led to today's most important environmental issue, namely wastewater, causing severe problems to humans, animals, and the environment.[1-3] Wastewater is a collection of water generated by homes, industries, and businesses, containing pollutants, including organic matter, nutrients, bacteria, viruses, pharmaceuticals, and other toxins.[4-6] Exposure to these pollutants can cause illness in humans and animals and environmental issues. Fortunately, wastewater is composed of several reusable components, and, for example, water, phosphorus, nitrogen, and carbon can be recycled.[7-9] Thus, the appropriate treatments to recycle such pollutants must be implemented to achieve clean water acceptable for loading back into the environment. Furthermore, the conventional, alternative, and emerging technologies and processes should focus on improving resource recovery, minimizing the carbon footprint, and pushing to be more self-sustainable and eco-friendly.

In the past, when waste was added directly into rivers, lakes, and bogs, the natural process of purification began.[10] Due to the sheer volume of clean water alone, the waste was diluted enough to be considered safe. Additionally, bacteria and plants in the water consume some pollutants, turning them into less harmful by-products.[11-13] Unfortunately, today's larger populations and greater demand for freshwater require mother nature to seek assistance from public works. This led to the use of the first sewer system in the US in the 1850s and then finally the first US sewage treatment plant by the 1890s.[14] Wastewater treatment consists of physical, biological, and chemical processes that safely generate clean water to reload into the environment.[15]

1.1.1. Conventional wastewater treatment

The term "conventional" refers to the societal development of the US. It is a relative term and is subject to change depending on geographic location. Federal government agencies govern conventional WWT technologies, rules, and regulations (e.g., EPA) to meet water quality standards of the "Safe Drinking Water Act". The process of treating wastewater in a modern WWT facility is categorized into four major stages: pretreatment, primary treatment, secondary treatment, and advanced treatment. The purpose of the pretreatment process is to block the introduction of pollutants, which may damage machinery/ equipment and interfere with the later WWT processes.[16] The primary treatment utilizes a series of physical processes (e.g., filters and sedimentation) to remove large floating objects, grit, and other organic and inorganic suspended solids.[17] During secondary treatment, the removal of most organic matter occurs through a biological process that utilizes microorganisms that consume biodegradable soluble organic contaminants.[18] Advanced or tertiary treatment is typically the final process, although not always required if an ecosystem is less sensitive, and uses treatment techniques to target specific pollutants and disinfect, typically leaving the water at a safe-to-drink level.[18]

1.1.2. Conventional disinfection

Due to the potential for ROS use for this step, the remainder of this chapter will focus on the disinfection step. The primary purpose of the disinfection step is to remove or kill any pathogenic microorganisms that were not removed during the primary and secondary stages.[6,18,19] Generally, there are two different methods of disinfection used: physical and chemical. The most commonly used method is chemical, in the form of chlorination. Chlorine is

a potent oxidizing agent that can oxidize most organic matter, react with bacteria cell walls and other vital cellular systems, and inactivate enzymes resulting in the inactivation or death of the pollutant.[20,21] These mechanisms of chlorine disinfection render the water safe for human consumption.

There are several chlorine species, which are not equally as effective as disinfectants. The effectiveness of species is influenced by two factors: cell penetration/diffusion rate and reactivity with the cell wall, proteins, and organics.[22,23] Chlorine gas (Cl_2) is the most cost-effective species used in WWT; unfortunately, it is hazardous for handling and storage, resulting in the need for additional safety procedures. Therefore, other species have been used as disinfectants, for example calcium hypochlorite ($Ca(OCl)_2$) and sodium hypochlorite (NaOCl). Both hypochlorite salts have similar advantages and limitations of their own. Sodium hypochlorite requires fewer safety procedures than Cl_2 but has a limited shelf life and a high chemical cost. Calcium hypochlorite is much more stable than sodium hypochlorite, allowing long-term storage, but is more expensive and may be explosive if mishandled.

When comparing the advantages and limitations of chlorine disinfection, the most notable considerations are that they are highly effective against most pathogens; however, they all form undesirable disinfection by-products (DBPs). DPBs are unwanted side products typically formed when chlorine reacts with organic matter, and include, but are not limited to, trihalomethanes (THMs) and haloacetic acids. The long-term exposure of DPBs leads to several health concerns, namely cancer, reproductive issues, congenital disabilities in infants, and complex mayhem on aquatic life.[24-26] As a result, alternatives for chlorine are of increasing importance as they provide the ability to reduce the amount of chlorine needed.

1.1.3. Alternative disinfection

Due to the increasing severity of the demand for freshwater, many scientists and companies have developed new and efficient technologies to circumvent the DBP problem. However, conventional physical and chemical alternatives, for example UV-radiation and ozonation, have limitations of their own.[27-29] UV radiation has no residual effects that can be harmful to humans or aquatic life, but is not as cost-effective as chlorination. Ozone is more effective than chlorine in destroying viruses and bacteria.[21,27] Still, it is not economical for wastewater with high levels of suspended solids, biochemical oxygen demand, chemical oxygen demand, or total organic carbon.

1.1.4. Advanced oxidative processes in disinfection

Developments in chemical disinfection methods for WWT have led to several processes and technologies that utilize advanced oxidative processes (AOPs).[29-31] Although there are vast amounts of AOPs, the remainder of this thesis will focus on photochemical technologies, which specifically involve photocatalysts or PSs. PSs have become more attractive than conventional WWT technologies for pollutant removal and disinfection because the technology is simple, clean, cost-effective, and energy-efficient. The mechanism used to explain the efficacy of light-activated AOPs is the generation of reactive oxygen species (ROS). Either direct or indirect photolysis can generate ROS. An example of direct photolysis is the irradiation of hydrogen peroxide (H_2O_2) to generate the hydroxyl radical (•OH).[32] In direct photolysis of the pollutants, the targeted pollutant must absorb the radiation and undergo degradation. Alternatively, indirect photolysis works by irradiating a PS, which absorbs a photon and results in populating an excited state, followed by energy transfer (ET) to molecular oxygen and generation of the

ROS. Subsequently, the ROS reacts with the pollutant, leading to either organic inactivation or cell death.[32]

The photosensitization process responsible for the generation of ROS can be explained by the Jablonski diagram shown in Scheme 1. Upon the population of the PS's excited singlet state, ^1S, from light irradiation ($h\nu$), subsequent intersystem crossing (ISC) populates the excited triplet state, ^3T, a state that is longer-lived and lower in energy than ^1S. From the ^3T state, ET to molecular oxygen (O_2) may occur, generating SO. The efficiency of this process is not only governed by the ET from the ^3T, but also the efficiency of the ISC. Using heavy atoms optimizes ISC efficiency via the heavy atom effect (HAE), which is a widely adopted approach that leads to a significantly increased ISC via enhancing spin–orbit coupling.[33,34] HAE can be achieved by complexing PSs to heavy atoms like lanthanide ions (Ln^{3+}). Depending on the relative positions of the PSs excited states, ET to the emissive excited state of the Ln^{3+} ion (f^*) can occur, and the return to the ground state (f) leads to Ln^{3+}-centered luminescence. However, this luminescence is competitive to SO generation and, therefore, decreases the efficiency of the photosensitization process. Using a heavy atom with emissive energy levels higher than the ligand ^3T state, such as gadolinium (Gd^{3+}) for example, that has an emitting level at 312 nm, prevents this ET to the Ln^{3+}, allowing for increased SO generation.[35] Other energy pathways that can occur are ligand fluorescence (Fl), phosphorescence (Ph), or non-radiative decay (NR) – all of which will decrease SO generation and are undesirable for applications in WWT.

Due to the promising applications of using light to generate ROS, several groups have investigated different PS materials. A blossoming topic in WWT is the use of peracetic acid (PAA).

PAA is used in AOPs to generate ROS. Therefore, PAA in WWT is promising in terms of implementation in the industry. According to Xiu-Wei Ao and collaborators,[30] a few research topics still need to be explored before PAA can make its industrial debut in WWT, including (1) cost-effective/ environmentally friendly activation, (2) ability to degrade several contaminants or inactivate microorganisms, (3) scalability, (4) environmental impact, including the impact of side products, and (5) potential removal of the side products and its recyclability. These five topics listed above are not exclusive to PAA but any material that generates ROS with applications in WWT.

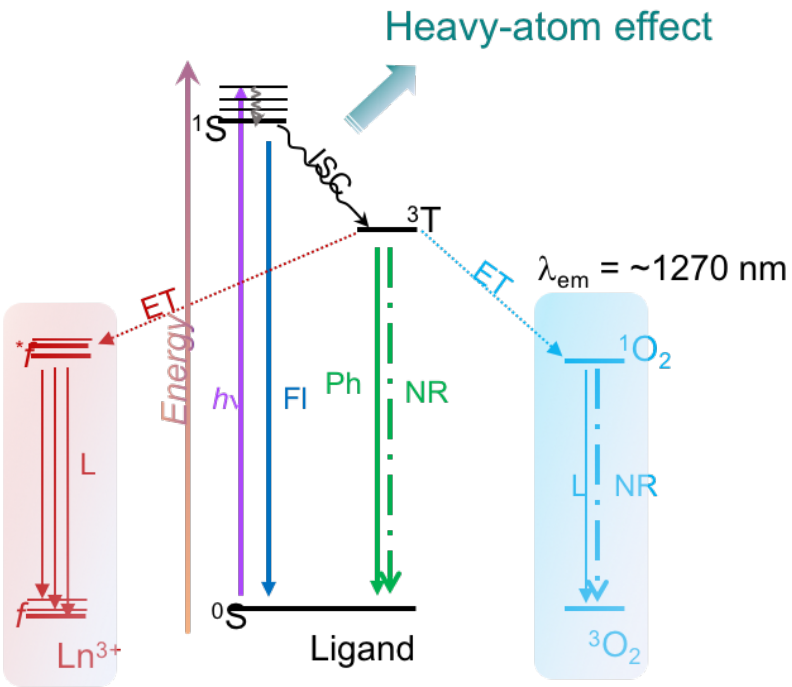

Scheme 1. Energy level diagram illustrating the competitive ET processes for Ln^{3+} sensitization and SO generation. Energy hυ is absorbed by the ligand and populates a singlet excited state (^1S). A triplet excited state (3T) is populated after intersystem crossing (ISC). ^3T can either ET to the emissive f* excited state, which decays by luminescence (L) to the ground state or ET to molecular oxygen. Other possible radiative processes are fluorescence (Fl) and phosphorescence (Ph). Energy levels are not drawn to scale.

1.2. Problem statement

At the rate natural resources are dwindling, the population is growing, and energy is consumed, significant advancements in global sustainability must be implemented. Water is the most critical resource and is required for all living things to exist. Therefore, conventional WWT must continue to evolve with more sustainable technologies to achieve the societal goals of the world.

1.3. The objectives of this work

This work aims to explore new materials that can be implemented in WWT, specifically the disinfection process. These processes and materials are simple, clean, cost-effective, and energy-efficient. This work will help push the importance and practicality of implementing more sustainable WWT technologies and techniques. We have

1. designed and characterized new PS-doped membranes that generate SO.
2. determined the ability of these PS-doped membranes to degrade pollutants.
3. determined the stability of these PS-doped membranes in water.
4. gathered preliminary data on PSs that can used to design new metal-organic frameworks (MOFs) that generate SO.

In the continuation of this work, we propose to exploit the potential of MOFs as SO generators in WWT.

1.4. Organization of this work

Chapter 1 contains an introduction to WWT, conventional WWT technologies, and new emerging technologies. Chapter 2 presents data on PS-doped membranes that have been shown to degrade model pollutants found in wastewater. Chapter 3 discusses a specific material that is classified as a metal-organic framework. Finally, chapter 4 summarizes the

principal findings and discusses further studies to ensure these light-activated materials can be implemented into the industry.

Chapter 2 - Photosensitizer doped membranes and the degradation of pollutants

2.1. Introduction

PSs generate SO upon irradiation with sunlight or artificial light sources.[32,36,37] SO is a ROS that can form endoperoxides with organic molecules, typically via a Diels-Alder type mechanism.[38-40] This enables the degradation of pollutants, viruses, and bacteria. Oxidation of substrates by SO is biologically noninvasive, eco-friendly, and cost-effective with diverse applications from photodynamic therapy to WWT.[41-44]

To address global environmental concerns over water quality, the removal of organic pollutants from water sources needs to be optimized.[45] In water treatment facilities, treatment with chlorine is typically the last step of the disinfection process before loading back into the environment. The drawback with using chlorine is the production of DBPs, for example, THMs.[21] The long-term exposure of THMs leads to several health concerns, namely cancer, reproductive issues, congenital disabilities in infants, and complex mayhem on aquatic life.[24-26] As a result, alternatives for chlorine are of increasing importance as they provide the ability to reduce the amount of chlorine needed.

Ideally, an eco-friendlier process would be implemented into WWT, for example in the form of photoactive coatings. Unfortunately, photoactive coatings capable of disinfecting wastewater to a "safe to drink" level have not been reported.[46] In an approach to developing such coatings, we have doped membranes with PSs that are known to generate ROS, specifically SO.[47-

[49] These membranes have the potential to be applied as surface coatings in WWT facilities, to reduce the amount of chlorine needed.

We describe the synthesis and characterization of three new functionalized membranes that generate SO and deactivate a model pollutant commonly found in wastewater, propranolol.[50-52] We doped Clear Flex 50 (CF50), an optically transparent, flexible, and commercially available polymer with three PSs (see Scheme 2), namely terthiophene (3T), a natural SO generator, Nap-cbx, and $[Gd(Nap\text{-}cbx)_3](NO_3)_3$, which were developed by our group and shown to generate SO efficiently.[53] We found that the functionalized membranes generate SO when irradiated with UV and visible light. Degradation studies of the model pharmaceutical propranolol by these membranes were conducted. The stability of the membranes was investigated by monitoring changes in the emission intensity of the doped PS, in the SO generation as monitored by its emission at 1277 nm, and in the membranes' ability to degrade propranolol after repeated use.

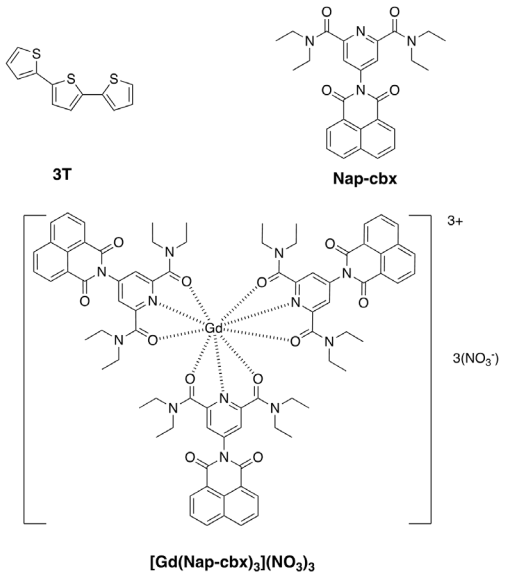

Scheme 2. 2,2′:5′,2′′-Terthiophene (3T), Nap-cbx, and $[Gd(Nap\text{-}cbx)_3](NO_3)_3$ used as photosensitizers.

2.2. Experimental

2.2.1. Materials

All commercially obtained reagents were of analytical grade and were used as received. Solvents were dried and purified by standard methods unless otherwise noted. The CF50 liquid rubber was purchased from SMOOTH-ON, and membranes were prepared as suggested by the manufacturer. The model pharmaceutical, DL- propranolol hydrochloride, 99% was purchased by Acros Organics. The 1-mL ampule of Megamix – 8270 was purchased from Restek. Nap-cbx and $[Gd(Nap\text{-}cbx)_3](NO_3)_3$ were synthesized as indicated in Scheme 3 following a modified literature procedure.[53] All synthetic steps were completed under N_2 unless otherwise specified. All photophysical and degradation data presented in this work are the average of at least three independent measurements. All stock solutions and reaction solutions were prepared using ultrapure water (18 MΩ) from a Thermo Barstead Nanopure Water Purification System Model 7146.

2.2.2. Synthesis of Nap-cbx

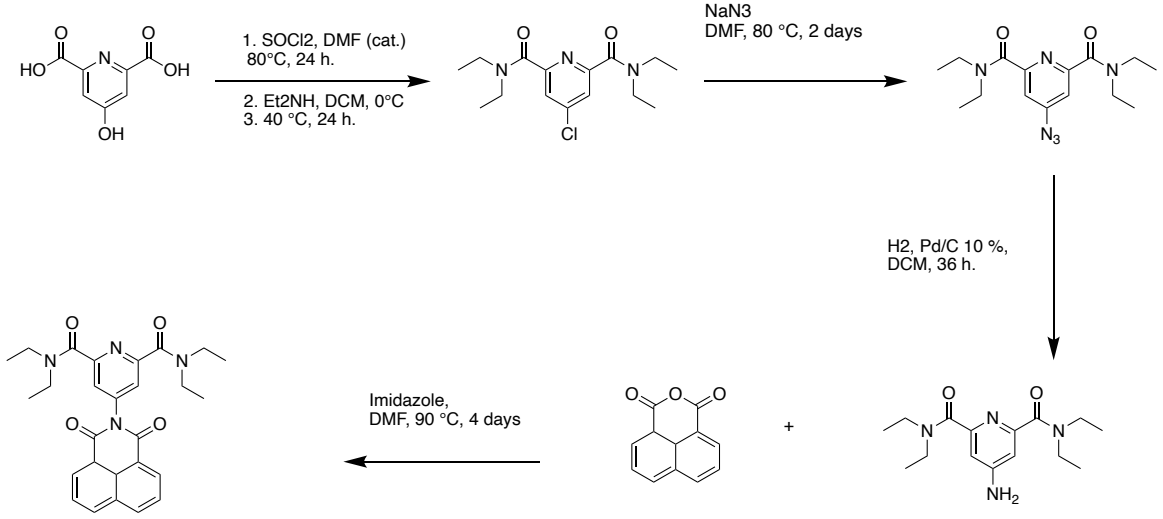

Scheme 3. Synthesis of Nap-cbx modified from [53].

Synthesis of Nap-cbx according[53] to a modified literature procedure consisting of different solvents, higher reaction temperatures and longer reaction times. 1,8-Naphthalic anhydride (5) (677.8 mg, 3.420 mmol), imidazole (2.3282 g, 34.20 mmol), and (4) (1000 mg, 3.420 mmol) were dissolved in dry DMF (30 mL) and refluxed for 4 days. The reaction was cooled to room temperature and quenched with 1M HCl. The reaction mixture was extracted with $CHCl_3$ (3 x 50 mL) and washed with water (3 x 50 mL) and brine (3 x 50 mL). The combined organic layers were dried over Na_2SO_4 and filtered. The solvent was removed under reduced pressure, and the product was isolated as a white solid. The crude material was purified using flash chromatography on silica using ethyl acetate as the eluent. Yield: 1.075 g, 67%. 1H-NMR (400 MHz, chloroform-d) δ 8.65 (dd, J = 7.3, 1.1 Hz, 1H), 8.34 – 8.29 (m, 1H), 7.82 (dd, J = 8.3, 7.2 Hz, 1H), 3.58 (q, J = 7.1 Hz, 2H), 3.44 (q, J = 7.0 Hz, 2H), 1.25 (dt, J = 12.0, 7.1 Hz, 6H).

2.2.3. Membrane preparation and doping

CF50 is a commercially available optically transparent, flexible, and UV-resistant polymer. It is obtained as a two-component elastomeric polyurethane with part A (an isocyanate) and part B (a polyurethane), by mixing A and B with a weight ratio of A: B = 1:2.

The doping of the films was achieved by adding the uncured polymer to varying amounts of the PS 3T, Nap-cbx, or $[Gd(Nap\text{-}cbx)_3](NO_3)_3$, dissolved in an anhydrous solvent (toluene or MeCN) under an inert atmosphere. First, the PS-doped polymer mixture was degassed under reduced pressure for 5 minutes. Next, the polymer was drop cast (0.60 mL) into a homebuilt round Teflon mold (13 mm diameter). To remove gas bubbles trapped inside the liquid rubber, the polymers in the molds were degassed under reduced pressure in a desiccator then heated in an oven to 72°C for 16 hours.

2.2.4. Scanning electron microscopy (SEM)

Secondary electron imaging was performed on a JEOL 7100FT field emission scanning electron microscope in the Mackay Microbeam Laboratory at the University of Nevada, Reno. Samples were coated with a ~2 nm thick iridium layer on a Leica ACE600 coater. The electron beam was set to 5.0 kV accelerating voltage and a working distance of 10 mm.

2.2.5. Spectroscopic measurements

Luminescence spectra of 3T-, Nap-cbx-, and $[Gd(Nap\text{-}cbx)_3](NO_3)_3$-doped CF50 membranes were obtained on a Fluorolog-3 fluorimeter (Horiba FL3-22-iHR550), with a 1200 grooves/mm excitation monochromator with gratings blazed at 330 nm, and 1200 grooves/mm or 600 grooves/mm emission monochromator with gratings blazed at 500 or 1000 nm for UV−vis or NIR range, respectively. An ozone-free xenon lamp of 450 W (Ushio) was used as the radiation source. The emission spectra were measured in the range 350−800 nm using a Hamamatsu 928P detector and in the range 800−1600 nm using a Hamamatsu 5509−73 detector cooled with liquid N_2. In addition, emission spectra of propranolol were measured on a Perkin-Elmer LS-55 with slit widths for emission and excitation of 2.5 nm, scan rate of 50 nm/min, and gain of 650 V. All emission and excitation spectra were corrected for instrumental function. Unless otherwise indicated, all measurements were performed at 25.0 ± 0.1 °C.

2.2.6. Degradation of propranolol and membrane stability

A propranolol solution (40 mL, 98.0 μM) in contact with a PS-doped membrane was irradiated at either 365 or 400 nm for 24 hours (UVGL-25 compact UV lamp (irradiance = 3.0 mW/ cm^2) or homebuilt LED chamber (irradiance = 7.3 mW/ cm^2), and the emission of propranolol was monitored as a function of irradiation time (see Scheme 4). The UV light meter (LM-10HTD, Coherent, USA) was placed under the UV source at the same distance as the irradiation range (1

inch) used for the experiments, to obtain the intensity of UV lamp (3.0 mW/ cm^2). The visible light meter (S121B, 400-1000 nm, Thorlabs, Germany) was placed into the LED chamber at the same distance as the irradiation range (0.5 inch) used for the experiments, to obtain the intensity of the chamber (7.3 mW/ cm^2).

This experiment was repeated after the membrane was irradiated for 48 and 72 hours, assessing the effect of repeated use on the membrane's ability to degrade propranolol. For all photocatalytic experiments, light control experiments were performed by monitoring the emission of propranolol before and after the 24-hour irradiation cycle in the absence of the doped membranes.

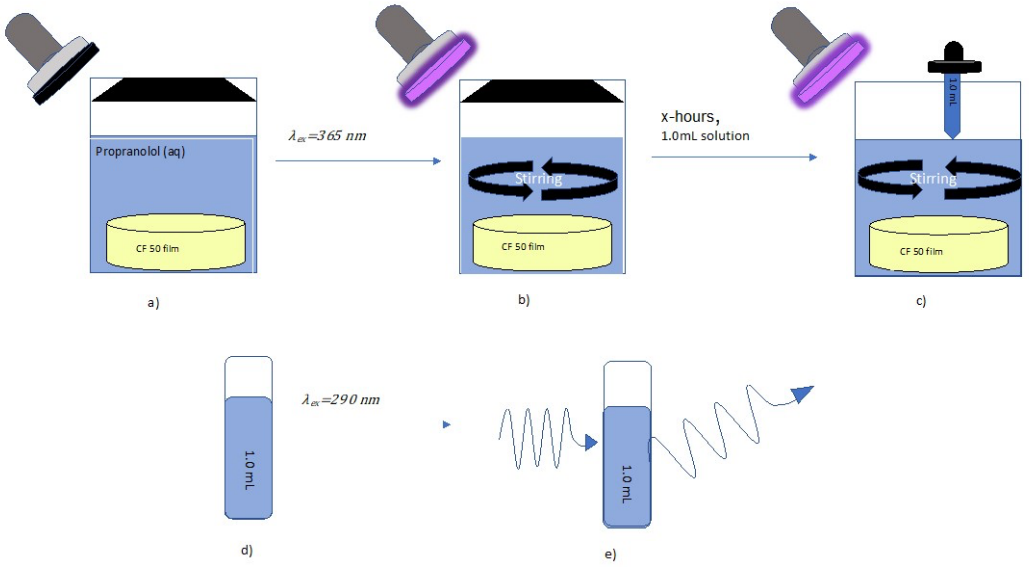

Scheme 4. Illustration of the setup used to monitor the degradation of propranolol. A) CF 50 membrane is submerged into a 40 mL of a 98.0 µM propranolol aqueous solution. b) While the propranolol solution stirring, the membrane is irradiated with 365 nm light using a handheld lamp (UVGL-25 compact UV lamp, 365 nm BLB, irradiance = 3.0 mW/cm^2). c) After 24-hours of irradiation, 0.6 mL aliquots are dispensed into cuvettes in the absence of light. d) The 0.6 mL aliquot is irradiated at 290 nm. e) The degradation is monitored by measuring the change in the emission of propranolol.

2.2.7. Degradation of Megamix

The ability of the doped membranes to degrade organic contaminants was analyzed by LC/MS, using an 8270 Megamix standard (Restek, Bellefonte, PA) containing 76 volatile and semivolatile organic pollutants (1 mg/mL of each contaminant). This standard, prepared in dichloromethane, was diluted in 15 mL of methanol and sonicated; the mixture was then added to ultrapure water to achieve target concentrations of 0.056 mg/L for each contaminant.

The Megamix solution (6 mL, 0.056 mg/L) in contact with the PS-doped membrane was irradiated for 24 hours (UVGL-25 compact UV lamp (irradiance = 3.0 mW/ cm^2) or homebuilt LED chamber (irradiance = 7.3 mW/ cm^2) and the intensity of select peaks in the chromatogram was monitored as a function of irradiation time. The membranes' degradation ability was evaluated based on the decrease in peak area of selected pollutants in the chromatogram. Two pollutants with retention times centered around 5 and 17 minutes were used, as their signals did not overlap with unexpected CF50 peaks.

2.2.8. LC-MS analysis of the samples

LC-MS was run on an Agilent Technologies, Inc. Model: 1200 Series HPLC with quat pump and DAD detector. TOF-MS make: Agilent Technologies, Inc. Model: G6230B Source: dual ESI G1969-65338. A C18 column (Agilent Technologies, Inc. 150 mm x 4.6 mm x 5.0 µm, stationary phase: Zorbax SB-C18, particle size: 5.0 µm, part number: 863953-902) was used with a mobile phase consisting of water, formic acid, and acetonitrile (14.9/0.1/85 %v/v/v), with a flow rate of 1.0 mL/min. Data collection and analysis software were Agilent Mass Hunter Workstation LC/MS data acquisition, version B.09.00. and Agilent Mass Hunter workstation

qualitative analysis, version 10.0. The propranolol and Megamix solutions were not pretreated and 10 µL aliquots were injected directly into the HPLC–MS system.

2.3. Results and discussion

2.3.1. Membrane doping and performance

We have synthesized several membranes doped with the PSs 3T, Nap-cbx, and $[Gd(Napcbx)_3](NO_3)_3$. The color and transparency of the membranes with all PSs at different concentrations are shown in Figure 1. Low concentrations of PS lead to colorless films. For each dopant, 3T, Nap-cbx, and $[Gd(Nap\text{-}cbx)_3](NO_3)_3$, the membrane takes on the color of the respective PS. While Nap-cbx membranes remain colorless, at high concentrations they are no longer transparent; a similar effect is seen for the Gd-based membrane. The doped filmed morphology was evaluated using scanning electron microscopy (SEM), which indicates that the membranes are nonporous (Figure 2). Comparison by SEM of the undoped to the doped membranes suggests that doping with the PS does not lead to differences in membrane morphology (Figure 2A-2D). EDS element mapping of the 1.75 % (w/w) $[Gd(Nap\text{-}cbx)_3](NO_3)_3$doped membrane (Figure 2E) shows Gd evenly distributed throughout the membrane, indicating that the doping of the membrane was successful.

The reflectance, excitation, and emission spectra of the three PS-doped membranes are shown in Figure 3. The 3T-doped membrane has a maximum excitation wavelength at 373 nm with an emission maximum of 431 nm. The Nap-cbx- and Gd-doped membranes have blue shifted excitation and emission, with maxima at 330 and 381 nm, respectively.

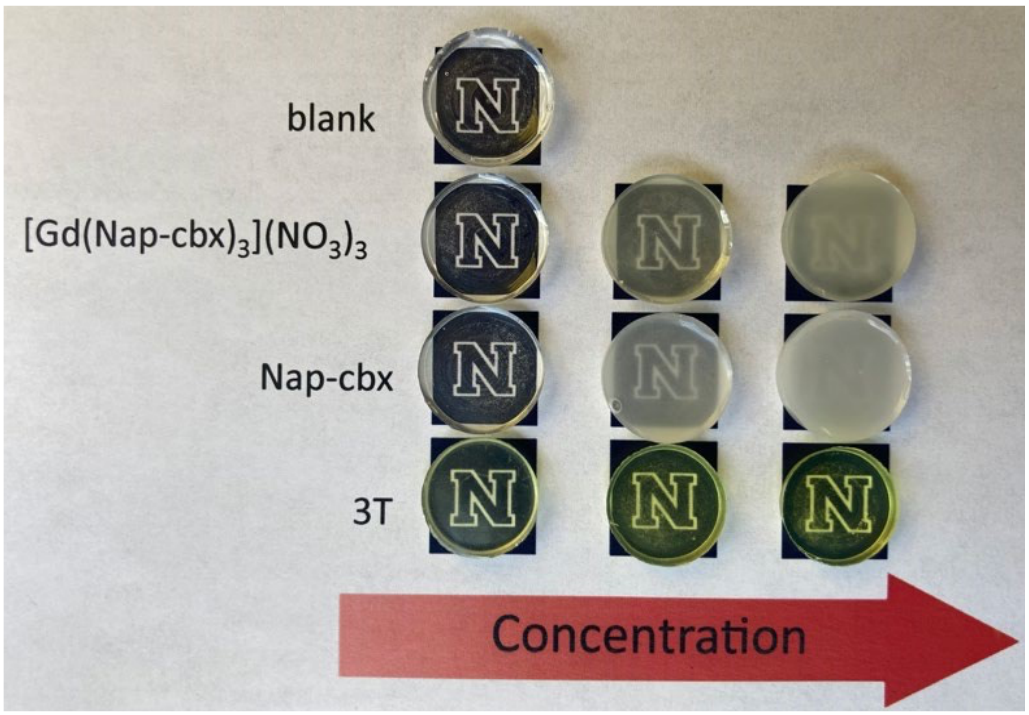

Figure 1. Photograph of an undoped membrane and CF50 doped with varying concentrations of 3T, Nap-cbx, and $[Gd(Nap\text{-}cbx)_3](NO_3)$.

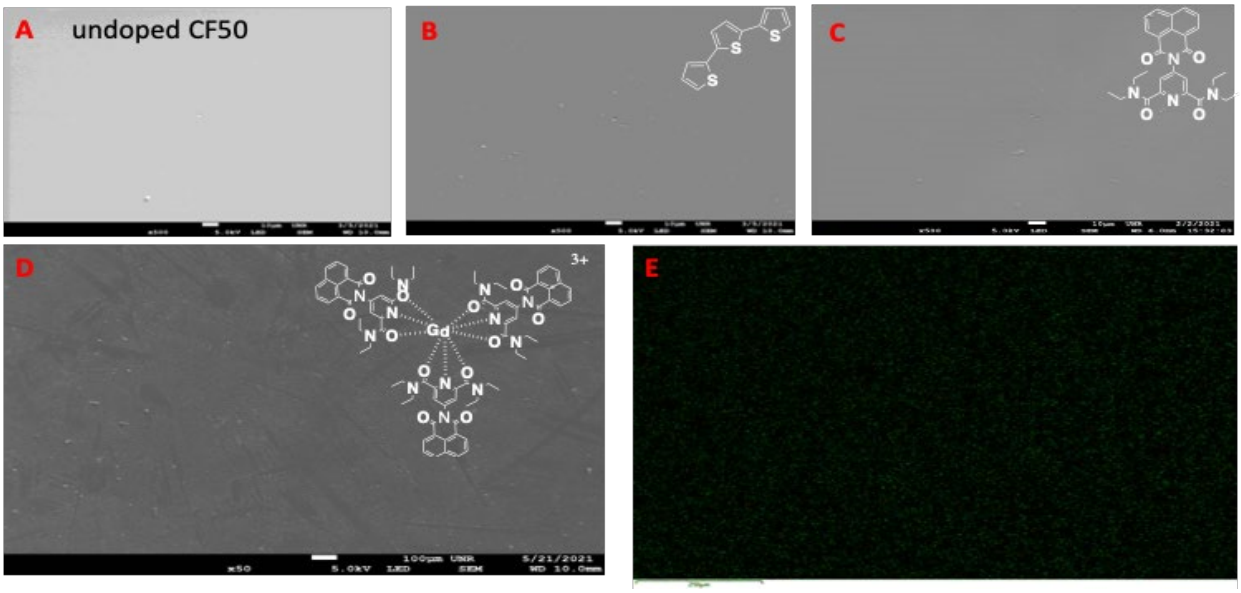

Figure 2. High resolution SEM micrographs of an (A) undoped Clear Flex 50 membrane, (B) 0.8 %(w/w) 3T-doped membrane, (C) 1.0 %(w/w) Nap-cbx-doped membrane, (D) 1.75 %(w/w) $[Gd(Nap\text{-}cbx)_3](NO_3)_3$-doped membrane, and (E) an energy dispersive X-ray spectroscopy (EDS) element mapping of Gd showing its distribution within the 1.75 %(w/w) $[Gd(Nap\text{-}cbx)_3](NO_3)_3$doped membrane.

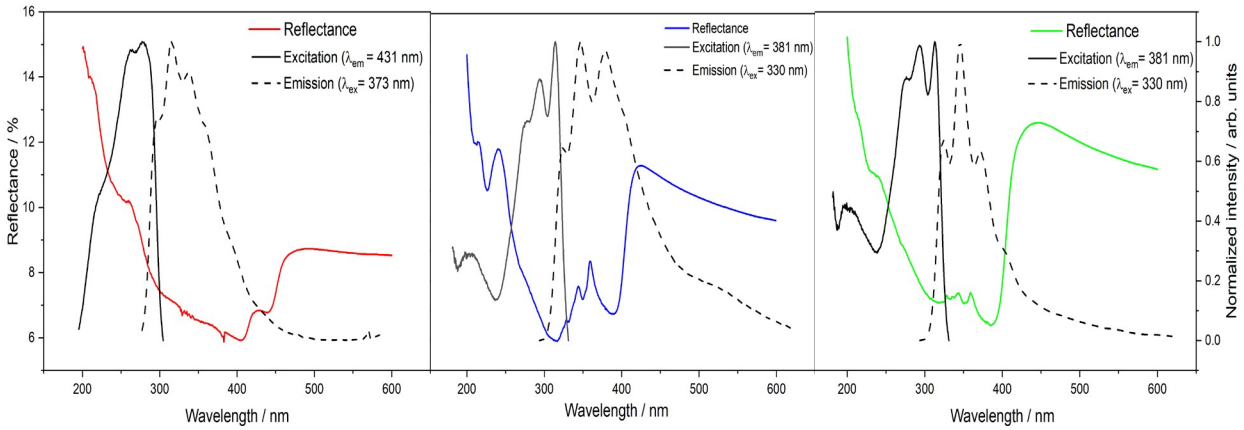

Figure 3. Normalized reflectance (colored), excitation (solid black), and emission (dashed) spectra of the three PS-doped membranes. Spectra displayed from left to right 3T, Nap-cbx, [Gd(Nap-cbx)$_3$](NO$_3$)$_3$.

2.3.2. Singlet oxygen generation

The ability of the membranes to generate SO was assessed by measuring the phosphorescence spectrum of SO at ~1280 nm. All three membranes generate SO, and Figure 4 shows the phosphorescence of SO. Using the same dopant concentration of 0.1%(w/w), the emission of SO was compared amongst the three membranes. Figure 4 shows that upon irradiating at 400 nm, the 3T-doped membrane generates the most SO. Irradiation at 350 nm of the Nap-cbx and [Gd(Nap-cbx)$_3$](NO$_3$)$_3$-doped membranes leads to less generation of SO. Figure 5 shows the excitation spectra monitoring the SO emission at 1277 nm for the three PS-doped membranes.

We have shown that all three PS-doped membranes generate SO; this led to our investigation on the dependence of SO generation on the PS concentration in the membrane. Plots of the SO emission intensity as a function of PS concentration (Figure 6) show an increase in SO generation with increasing amounts of 3T, Nap-cbx, and [Gd(Nap-cbx)$_3$](NO$_3$)$_3$ within the membranes. Plateaus for each PS are reached at 0.8, 1.0, and 1.75 %(w/w), respectively.

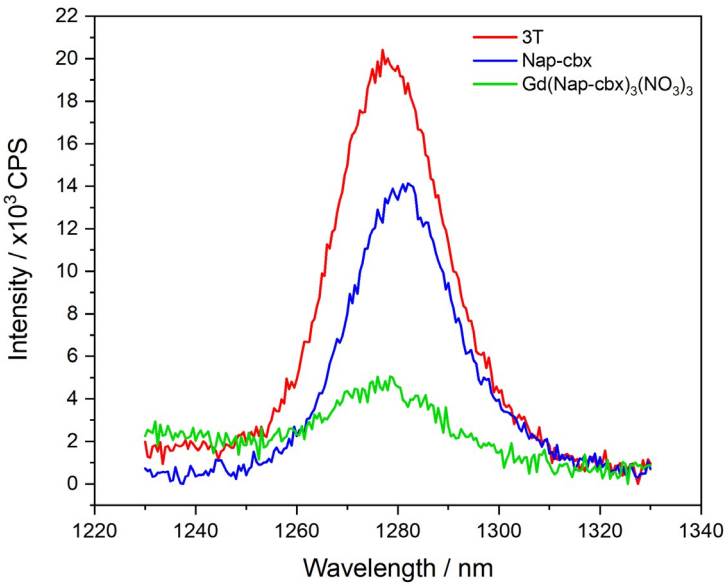

Figure 4. Phosphorescence spectra of SO generated by the doped membrane: 3T upon irradiation at 400 nm (red), Nap-cbx (blue), and $[Gd(Nap\text{-}cbx)_3](NO_3)_3$ (green) upon irradiation at 365 nm. [Dopant]= 0.1 %(w/w).

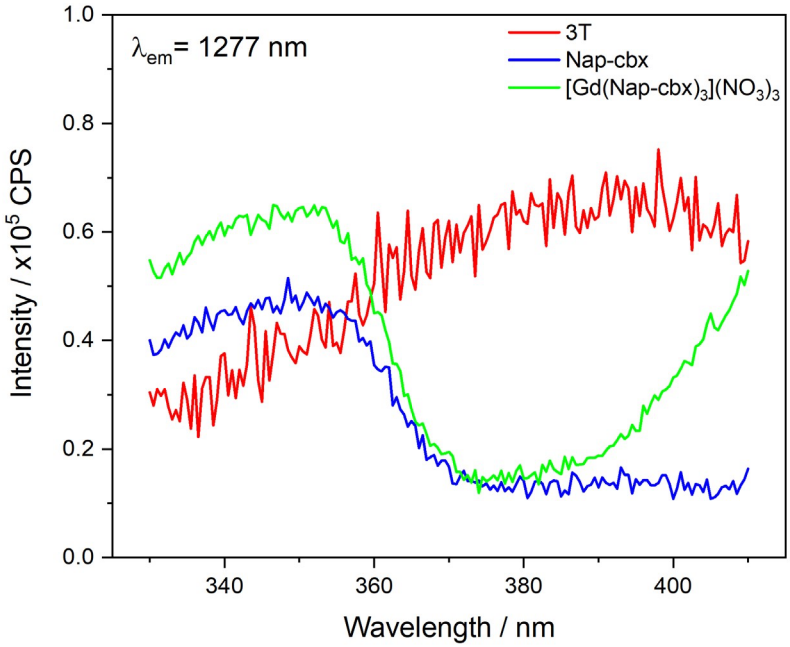

Figure 5. Excitation spectra of a 3T- (red), Nap-cbx- (blue) and a $[Gd(Nap\text{-}cbx)_3](NO_3)_3$-doped membrane (green) monitoring singlet oxygen emission at 1277 nm.

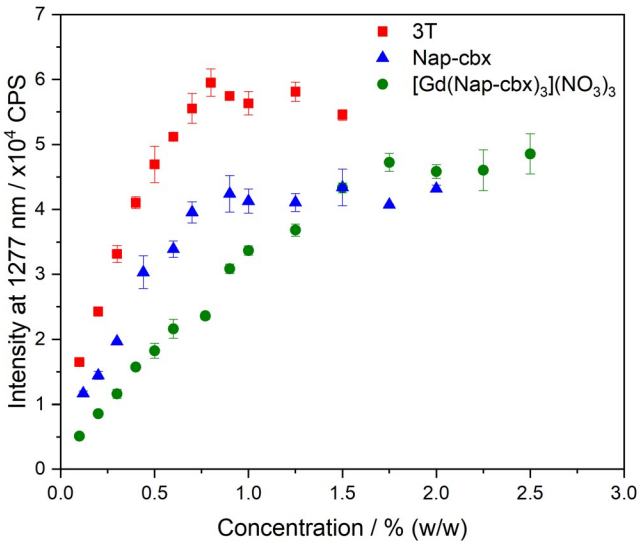

Figure 6. Intensity of SO emission at 1277 nm as a function of the concentration of 3T (red squares), Nap-cbx (blue triangles), and $[Gd(Nap\text{-}cbx)_3](NO_3)_3$ (green circles) in the CF50 membrane.

2.3.3. Degradation of propranolol

Propranolol is a beta-blocker, used for high blood pressure, chest pain (angina), and uneven heartbeat and is part of a class of water contaminants designated as a pollutant of emerging concern.[50,54,55] It absorbs at 290 nm and shows an emission maximum at 353 nm. To investigate the ability of our SO-generating membranes to degrade this model pollutant, we irradiated a solution of propranolol on its own (Figures 7 and 8) and when in contact with these PS-doped membranes (Figures 9-11). The Nap-cbx- and $[Gd(Nap\text{-}cbx)_3](NO_3)_3$-based membranes were irradiated at 365 nm, and the 3T-based membrane was irradiated at 400 nm, the excitation maxima for SO generation (Figure 5). In all cases, the emission intensity of propranolol showed an exponential decrease with irradiation time (Figure 12). Over 24 hours, decreases of 42, 36, and 41 %, for 3T, Nap-cbx and $[Gd(Nap\text{-}cbx)_3](NO_3)_3$, respectively, were observed.

In a complementary approach, the degradation of propranolol was investigated using LC/MS before and after 24 hours of irradiation in the presence of 3T-, Nap-cbx-, and $[Gd(Napcbx)_3](NO_3)_3$-based membranes (Figure 13). Analysis of the peak areas in the chromatogram indicates the decomposition of propranolol to be 65, 39, and 48% for the three membranes, respectively, consistent with the values obtained by fluorescence spectroscopy.

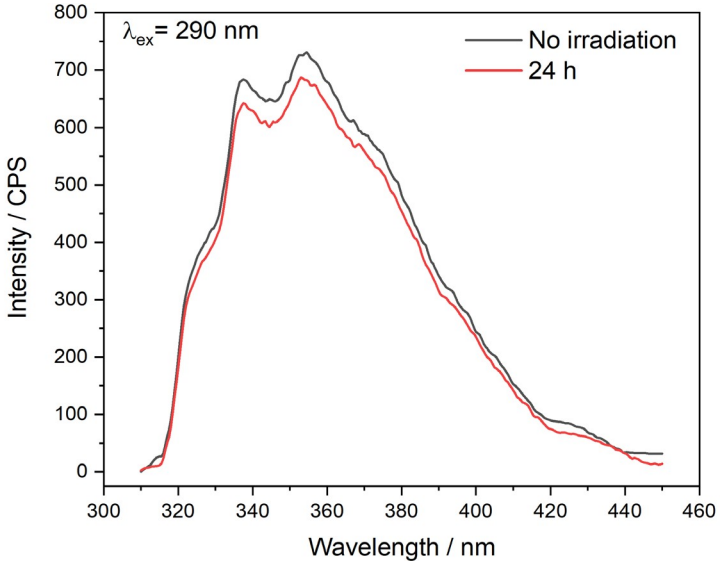

Figure 7. Emission spectra (λ_{ex}= 290 nm) of propranolol (40 mL, 98 μM) at 25.0°C in nanopure water after irradiating for 24 hours at 365 nm (3.0 mW/cm^2, UVGL-25 compact UV lamp) in the absence of a doped membrane.

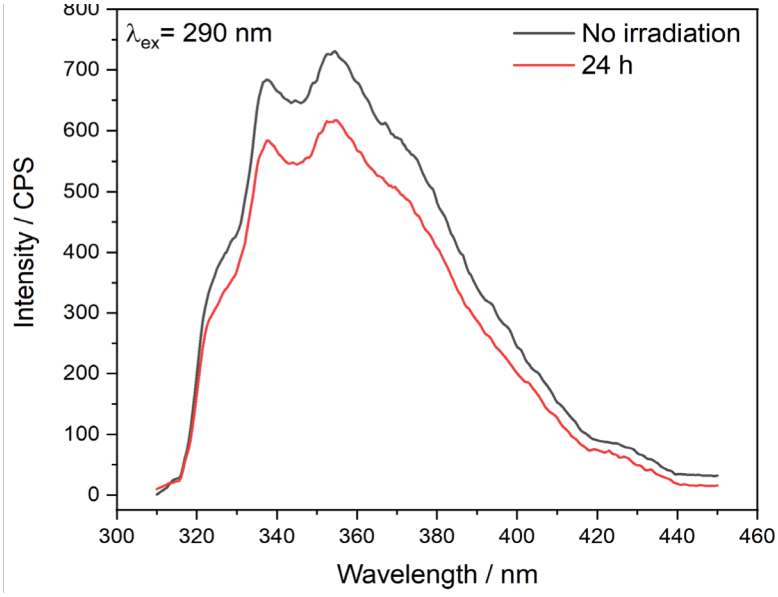

Figure 8. Emission spectra (λ_{ex}= 290 nm) of propranolol (40 mL, 98 µM) at 25.0°C in nanopure water after irradiating for 24 hours at 400 nm (7.3 mW/ cm^2 LED chamber) in the absence of a doped membrane.

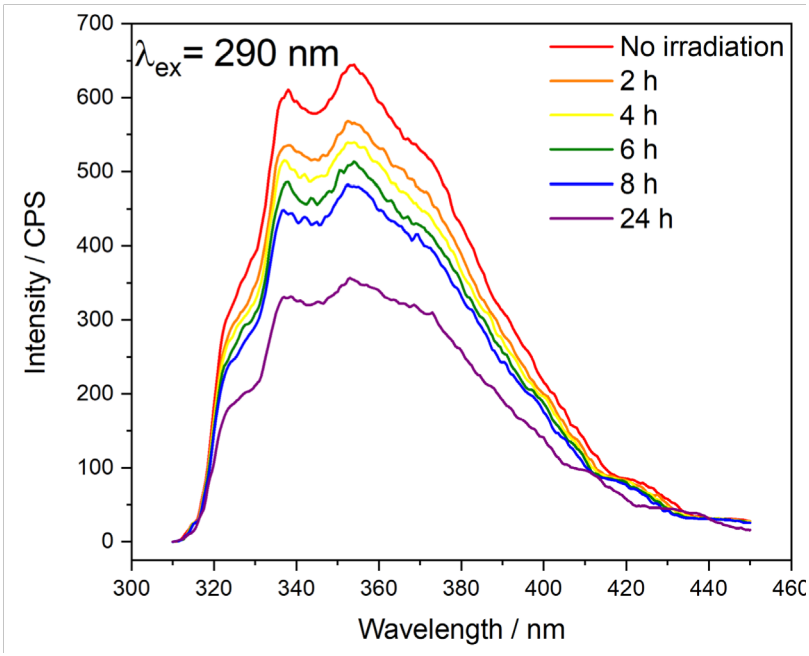

Figure 9. Emission spectra (λ_{ex}= 290 nm) for the first trial of cycle 1 of propranolol (40 mL, 98 µM) in nanopure water after irradiating with 400 nm (7 mW/ cm^2 LED chamber) at selected intervals in the presence of 0.8 %(w/w) 3T-doped membrane.

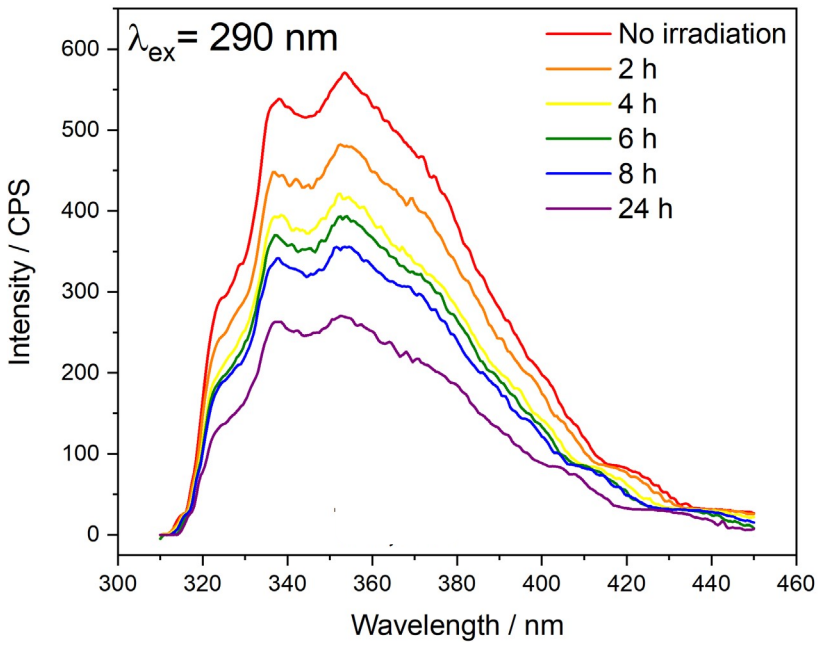

Figure 10. Emission spectra (λ_{ex}= 290 nm) for the first trial of cycle 2 of propranolol (40 mL, 98 μM) in nanopure water after irradiating with 365 nm (3 mW/ cm^2, UVGL-25 compact UV lamp) light in the presence of a 1.0 %(w/w) Nap-cbx-doped membrane.

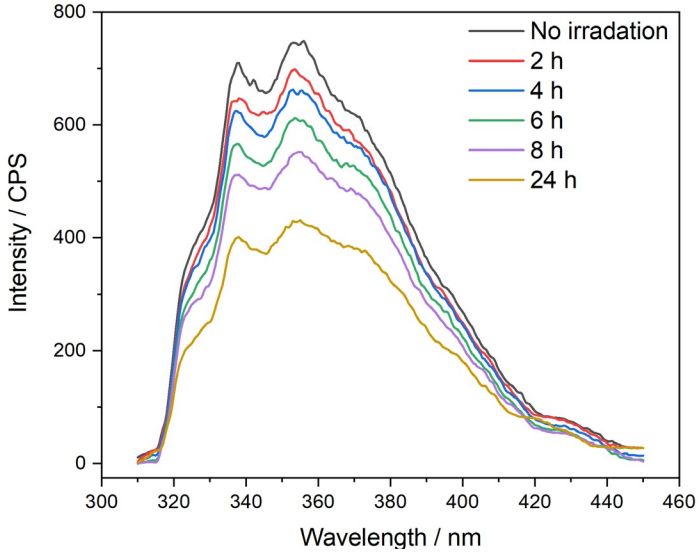

Figure 11. Emission spectra (λ_{ex}= 290 nm) for the first trial of cycle 1 of propranolol (40 mL, 98 μM) in nanopure water after irradiating with 365 nm (3 mW/ cm^2, UVGL-25 compact UV lamp) light in the presence of a 1.75 %(w/w) $Gd(Nap\text{-}cbx)_3(NO_3)_3$-doped membrane.

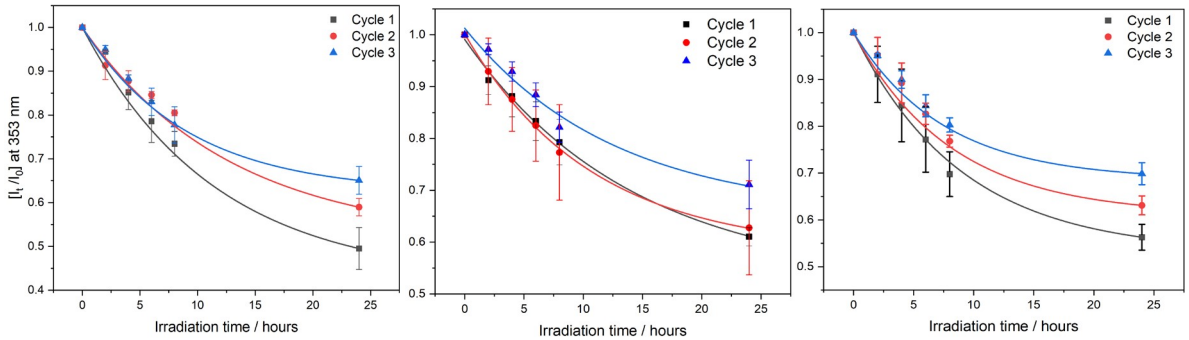

Figure 12. Plots of 3 24-hour cycles showing the emission intensity of propranolol at 353 nm as a function of irradiation time, from left to right, 0.8 ,1.0, 1.75 %(w/w), 3T, Nap-cbx, and $Gd(Nap\text{-}cbx)_3](NO_3)_3$-doped membrane, respectively (λ_{irrad} = 365 or 400 nm), Cycles 1-3

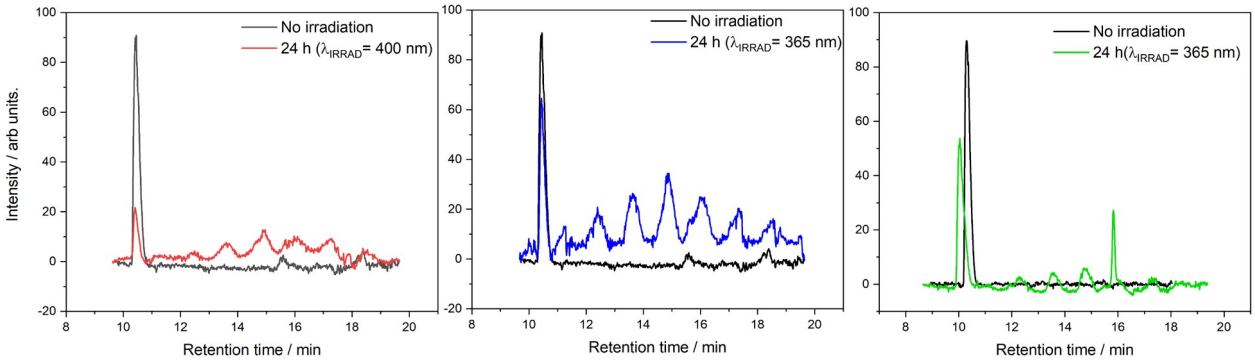

Figure 13. LC/MS analysis of a propranolol solution after 24 hours of irradiation (365 or 400 nm, colored) compared to a solution of non-irradiated propranolol (black). The degradation was performed using a 1.75 %(w/w) $[Gd(Nap\text{-}cbx)_3](NO_3)_3$-doped membrane.

2.3.4. Degradation of Megamix

The ability of the doped membranes to degrade organic pollutants found in Megamix was investigated by monitoring peak intensity changes in the chromatogram before and after irradiation. Figure 14 shows a chromatogram of a Megamix solution (0.056 mg/L of each contaminant) before irradiation (shown in black), Megamix after 24 hours of irradiation at 400 nm (shown in red), and Megamix after 24 hours of irradiation at 400 nm in the presence of a 0.8 %(w/w) 3T-doped membrane (shown in green). Two pollutants with retention times centered at 5 and 17 minutes have been highlighted in yellow. The two highlighted areas corresponding to the two chosen reference pollutants are magnified to show the decrease in the peak intensity, indicating degradation of the pollutant. Nap-cbx and $[Gd(Nap\text{-}cbx)_3](NO_3)_3$ -doped membranes were also screened for their ability to degrade Megamix (Figures 15 and 16), the data shows a degradation trend similar to the 3T-doped membrane.

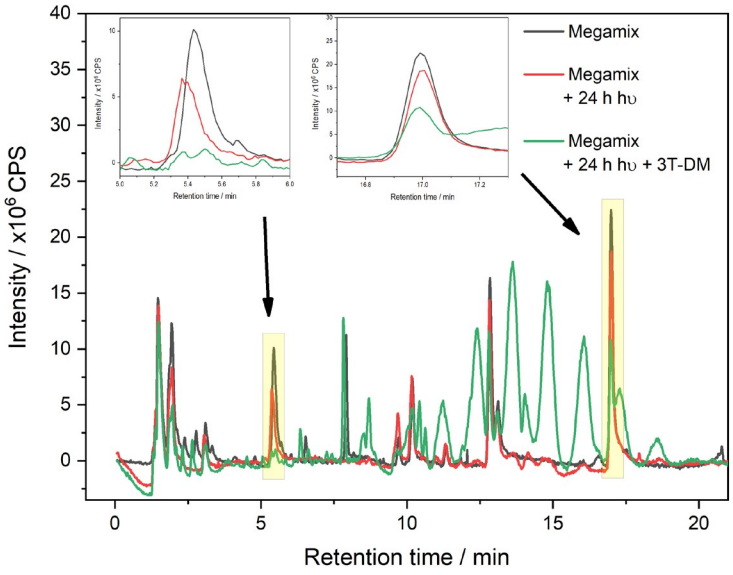

Figure 14. LC/MS analysis of Megamix (black), Megamix under 24 hours irradiation (red), and Megamix under 24 hours irradiation in the presence of a 0.8 %(w/w) 3T-doped membrane (3TDM) (green). The two inserts show magnified areas of the pollutants at 5 and 17 minutes. Irradiation= 400 nm (7.3 mW/ cm^2); [Megamix]= 0.056 mg/L

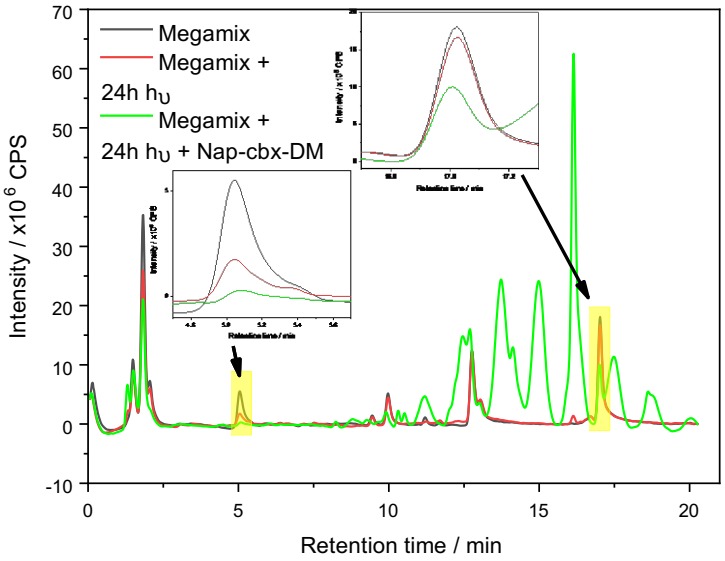

Figure 15. LC/MS analysis of Megamix (black), Megamix under 24 hours irradiation (red), and Megamix under 24 hours irradiation in the presence of a 1.0 %(w/w) Nap-cbx-doped membrane (Nap-cbx-DM) (green). The two inserts show magnified areas of the pollutants at 5 and 17 minutes. Irradiation= 365 nm (3.0 mW/ cm^2); [Megamix]= 0.056 mg/L

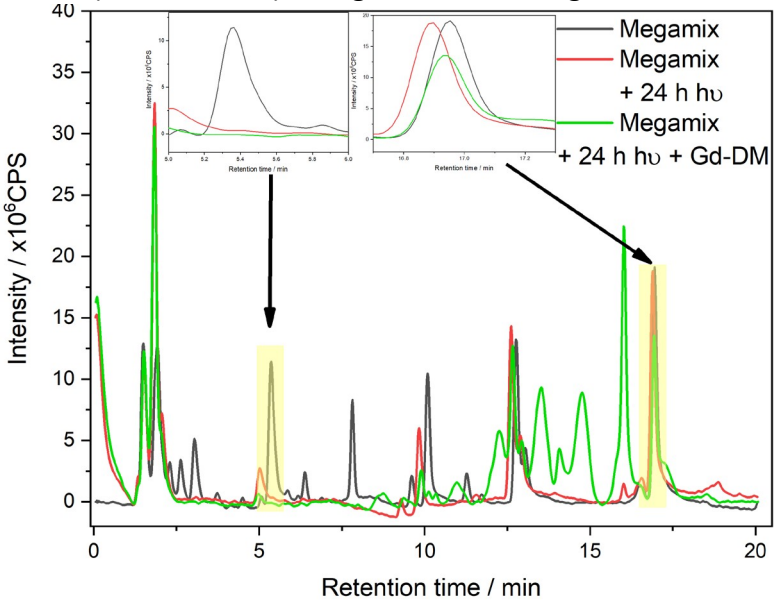

Figure 16. LC/MS analysis of Megamix (black), Megamix under 24 hours irradiation (red), and Megamix under 24 hours irradiation in the presence of a 1.75 %(w/w) $[Gd(Nap\text{-}cbx)_3](NO_3)_3$-

doped membrane (Gd-DM) (green). The two inserts show magnified areas of the pollutants at 5 and 17 minutes. Irradiation= 365 nm (3.0 mW/ cm^2); [Megamix]= 0.056 mg/L

2.3.5. Membrane stability

To monitor the stability of the membranes, their ability to degrade propranolol was monitored as a function of 24-hour cycles. Upon subjecting the 3T-, Nap-cbx-, and [Gd(Nap-cbx)$_3$](NO_3)$_3$-doped membranes to three irradiation cycles and monitoring ability to degrade fresh solutions of propranolol, a slight decrease in performance, indicated by the change in slope of the fitted emission data, was observed from 42 to 30 %, 36 to 27 %, and 41 to 29, respectively (Figure 12).

The stability of the membranes was further evaluated by their ability to degrade Megamix after multiple irradiation cycles. Figures 17-19 show the chromatograms of Megamix in the presence of doped membranes after multiple irradiation cycles. When evaluating the performance of doped membranes, the pollutants corresponding to the retention time of 5 and 17 minutes will be used to qualitatively observe the performance of the membranes. Using the same two reference peaks at 5 and 17 minutes, we see little to no difference in the performance of the membrane to degrade these pollutants. It is evident based on the light control of Megamix irradiated at 365 nm, that the reference pollutant at 5 minutes is less photo-stable (Figures 15 and 16).

To further monitor the stability of the membranes, chromatograms of the liquid the membrane was submerged in were analyzed, before and after the 24-hour cycles. Figures 13-19 all show a Gaussian distribution of peaks centered around 15 minutes which is characteristic of the polymer leaching. It is known that synthetic polymer samples will typically contain a

distribution of chain lengths, as seen in Figure 13 (blue graph). To circumvent this leaching issue, the membranes were washed with copious amounts of water before and after each irradiation cycle; then chromatograms were compared to the pristine membrane (Figure 20). Figure 20 shows a decrease in the polymer peaks, suggesting the washing decreases the leaching. Figures 17-19 also show a significant reduction in the intensity of the Gaussian distribution of peaks centered at 15 minutes upon the washing of the membrane.

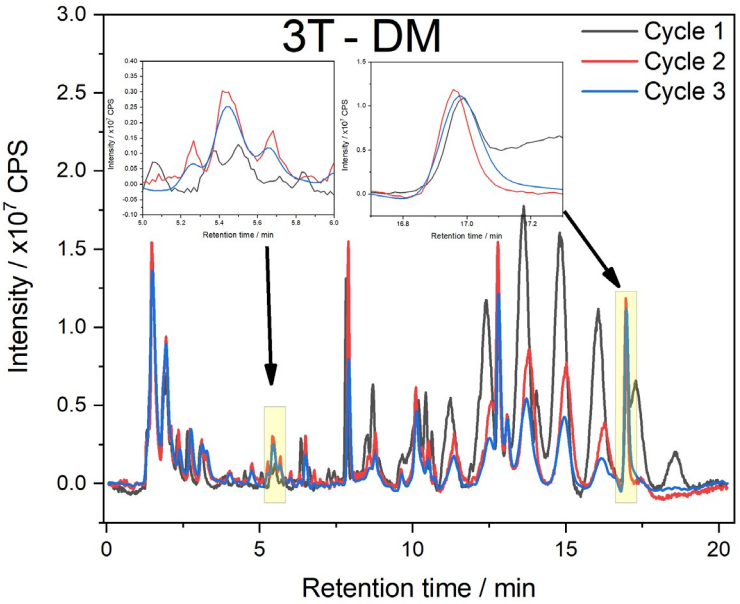

Figure 17. Plots of 3 24-hour cycles showing the intensity of the eluting bands of the components in Megamix as a function of irradiation time, using a 0.8 % (w/w) 3T-doped membrane. The two inserts show magnified areas of the pollutants at 5 and 17 minutes. (λ_{irrad} = 400 nm)

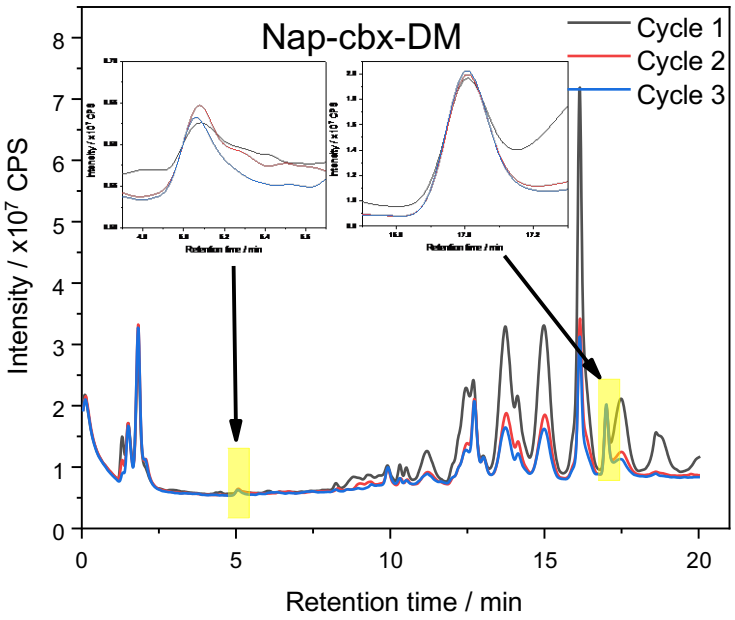

Figure 18. Plots of 3 24-hour cycles showing the intensity of the eluting bands of the components in Megamix as a function of irradiation time, using a 1.0 % (w/w) Nap-cbx-doped membrane. The two inserts show magnified areas of the pollutants at 5 and 17 minutes. (λ_{irrad} = 365 nm)

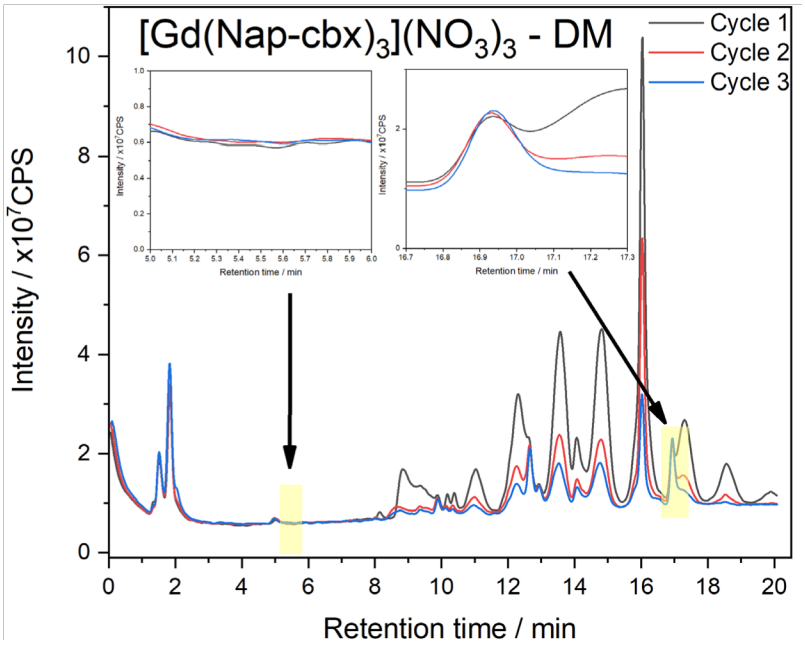

Figure 19. Plots of 3 24-hour cycles showing the intensity of the eluting bands of the components in Megamix as a function of irradiation time, using a 1.75 % (w/w) [Gd(Nap-cbx)$_3$](NO$_3$)$_3$ – doped membrane. The two inserts show magnified areas of the pollutants at 5 and 17 minutes. (λ_{irrad} = 365 nm).

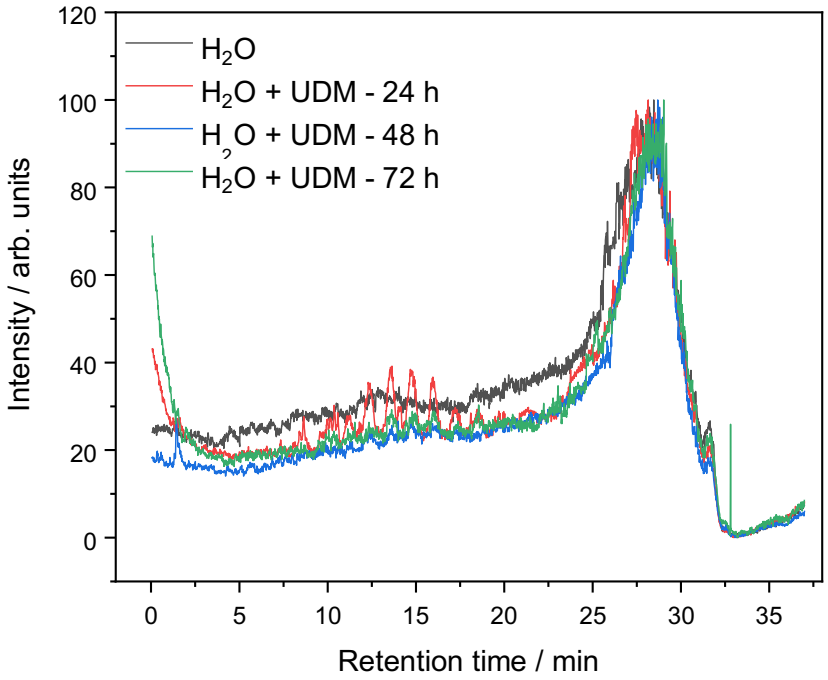

Figure 20. LC/MS analysis of water (shown in black) and water in the presence of CF50 after several hours of irradiation. Water in the presence of CF50 after 24 hours irradiation (shown in red), water in the presence of washed CF50 membrane after 48 hours irradiation (shown in blue), and finally water in the presence of a 2x washed CF50 membrane after 72 hours of irradiation (shown in green).

2.4. Summary

Three new PS-doped membranes were synthesized and explored for their ability to degrade the model pharmaceutical propranolol. We have seen that the membranes can photodegrade propranolol using UV and visible light as the irradiation source. Based on the change of propranolol's emission intensity, visible light performed the best for the 3T doped membranes. The ability of the Nap-cbx-doped membrane to degrade propranolol was enhanced upon the coordination of Nap-cbx to Gd. All three of the membranes were subjected to several cycles of the degradation of propranolol with minimal loss in performance.

All three doped membranes were screened for their ability to degrade several pollutants found in the standard 8270 Megamix. Using changes in chromatographic peak intensities, was shown that several pollutants degraded in the presence of these doped membranes, with little

to no loss in their performance over several cycles. Thus, these PS-doped membranes have demonstrated their potential for applications in wastewater treatment, and this work should help further the understanding of photo-activated materials used for water purification.

Chapter 3 - Metal-organic frameworks in WWT

3.1. Introduction

This chapter briefly introduces metal-organic frameworks (MOFs) and their design, synthesis, and application in WWT. MOFs, are a sub-class of coordination polymers and are porous solid-state materials consisting of inorganic metal-containing nodes bridged by organic ligands, referred to as linkers, forming one-, two-, and three-dimensional structures, as shown in Figure 21.[56-59] MOFs have the highest internal void volume of any material known to date, and have received much attention for purifications, separations, and storage.[32,46,56-60] Solid materials containing void spaces can act as molecular sponges. These sponges can selectively soak up gases, liquids, and solids, allowing for removing pollutants from water. The precise control or design of porous solids has been a long-standing challenge from a chemist's perspective.[56,60] It can be challenging to construct porous solids tuned for a particular application. Fortunately, MOFs can easily be modified by combining specific metals and organic molecules. Many groups have tackled this challenge with the construction of new MOFs.[31,48,58,61-64]

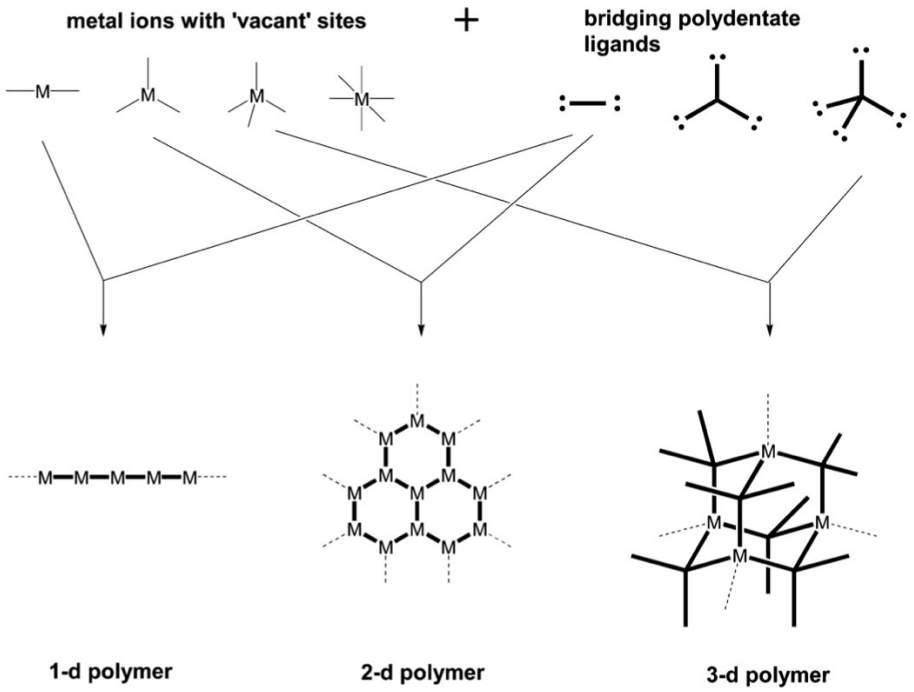

Figure 21. The building block, or modular, is the principle behind forming MOFs.[58]

This chapter discusses how design strategies of MOFs can be implemented to achieve select functionalities for advancing both the performance and fundamental understanding of light-activated materials used to enhance the WWT process. Using PSs as the organic linkers to construct photocatalytic MOFs that generate SO and adsorb pollutants is of great interest in WWT.[65] Photocatalytic MOFs have potential to be the leading technology for WWT and are the motivation behind the work described below.

3.1.1. Design of MOFs for WWT

Photodegradation and adsorption are two of the most sustainable technologies currently implemented in WWT.[48,56,60] However, these implemented processes remain to be separate techniques, that is why the design of efficient SO generating MOFs is of upmost importance.[66] The efficiency of a PS to generate SO is directly correlated to the singlet oxygen quantum yield (SOQY,Φ_{SO}).[32,65,67] It has been shown that increasing the conjugation of a PS or a linker by incorporating it into a network (e.g., formation of a MOF) is expected to improve

the SOQY and consequently enhance the degradation of pollutants.[65,68] In addition to enhancing SOQY upon forming these conjugated networks, there is also a red shift in the excitation wavelength needed to generate SO. Red-shifting in the excitation wavelength is beneficial for energy consumption as it requires lower energy photons to excite the PS. Ideally, a MOF used in WWT would have a high SOQY (value close to 1), using a broad range of visible excitation wavelengths (e.g., 400-700 nm) or the sun as irradiation source.[69,70]

Innovative approaches in MOF design allow for desirable properties such as porosity, structural morphology, recyclability, and thermal/chemical stability.[71] Some standard techniques used in MOF design are to vary the size and type of organic linker. For example, shorter rigid linkers exhibit more excellent thermal and chemical stability relative to longer flexible linkers. However, larger, more flexible linkers allow for higher porosity (larger internal void volume), resulting in better adsorption properties. According to V. Russo and others,[71] adsorption is a separation technique used for waste purification, which involves the selective interaction of one or more compounds in the liquid phase on a solid called the adsorbent. MOFs have many adsorption mechanisms (electrostatic, hydrogen bonding, acid-base, $\pi-\pi$ stacking, pore/size-selective, and hydrophobic interactions) that can be tuned for the selective removal of pollutants from wastewater.[71] The ideal properties of a MOF with application in WWT are large internal void areas and good thermally/ chemically stability. The ability of MOFs to adsorb selectively and photodegrade efficiently will allow for the sustainable removal of pollutants of emerging concerns that are difficult/impossible to remove with conventional WWTs.

3.1.2. Synthesis of MOFs

The term “simple,” as described in this section, is relative to the “one-pot” synthetic approach which there is no opportunity to adjust the MOFs properties post-formation. There are several strategies used in the construction of MOFs. Classical one-pot methods of coordinating clear solutions of the reactants can be used following the precipitation of the MOF upon heating or the passing of time. Another simple approach is using solvothermal chemistry, which involves mixing the reactants in a solvent then sealing them in a closed container (i.e., autoclave or pressure tube). Unlike simple solution approaches, the solubility of the reactants increases under solvothermal methods, which makes the reaction more likely to occur at lower temperatures. Small changes in one or more reaction variables, such as temperature, time, pH, or the solvent type, can profoundly influence the final product.[72] For both simple methods described above, achieving high purity MOF crystals with a narrow size distribution is possible. However, the synthesis and crystallization process remain an empirical process governed by the trial and error of various experimental conditions.[34]

3.1.3. MOF membranes for WWT

The end goal of a MOF designed for applications in WWT, is to use the MOF to clean water repeatedly with minimal loss in performance and uphold structural integrity. The two most rational design strategies for implementing MOFs into the WWT processes is to either incorporate them into a polymeric substrate (MOF-based composite membranes) or grow them onto a substrate (bare MOF membranes).[60,71] MOFs based membranes have been shown to have enhanced performance and stability relative to free MOFs.[60] A well-designed MOF membrane with applications in WWT must have high water stability, high SOQY, a large internal

void volume, and be constructed with the perfect combination of MOF synthesis and membrane manufacturing. However, according to Juan Li and others,[60] to uncover the full potential of the application of MOF membranes in WWT, several challenges need to be addressed. These challenges include the long-term stability of the MOF membrane in complex aqueous/organic solvent systems, acid/basic environments, and a wide range of temperatures. Additionally, scalability, societal acceptance, and environmentally friendly production must be considered to implement MOF membranes into the industry.

3.2. Experimental section

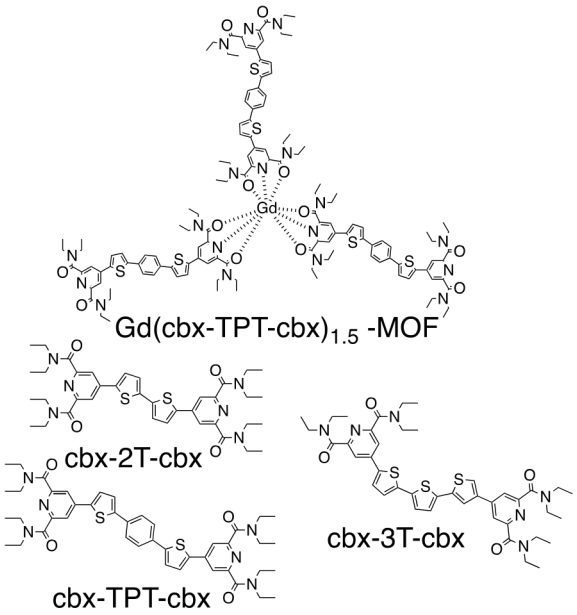

Scheme 5. Proposed $Gd(cbx\text{-}TPT\text{-}cbx)_{1.5}$ MOF, cbx-TPT-cbx, cbx-2T-cbx, and cbx-3T-cbx compounds described herein.

3.2.1. Crystallization of cbx-3T-cbx

The crystallization was performed by vapor diffusion. Cbx-3T-cbx (5 mg) powder was added to a 2-dram vial then dissolved in 2 mL of DCM. The 2-dram vial was placed in a 4-dram vial containing hexanes as the counter solvent, and after four weeks, orange needle-like crystals, shown in Figure 22, formed.

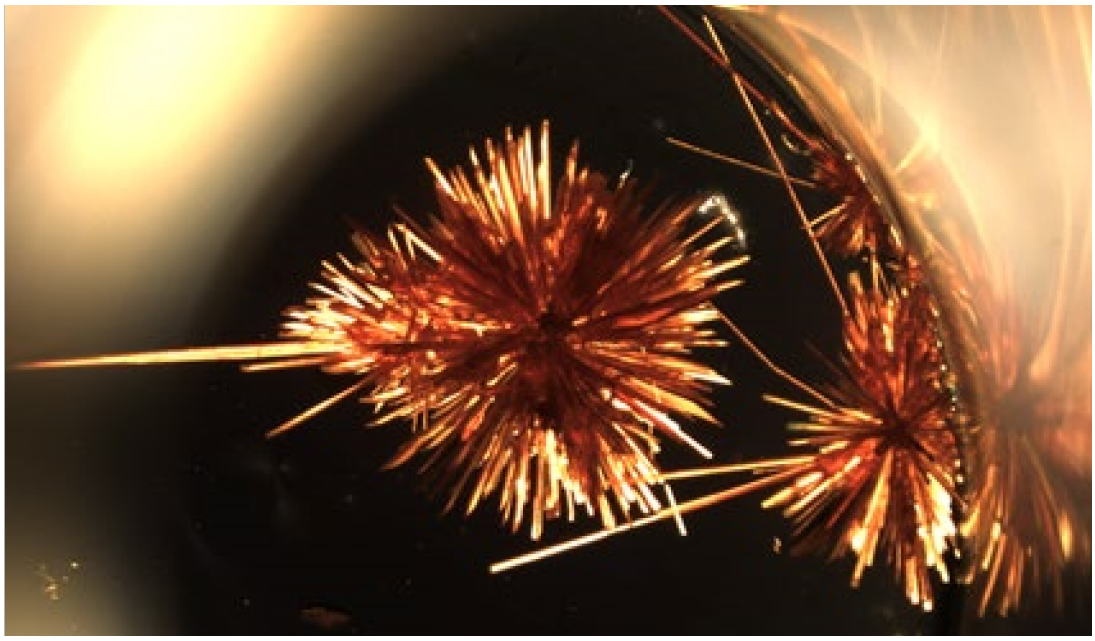

Figure 22. Photograph of the needle-like crystals obtained by the crystallization of cbx-3T-cbx powder.

3.2.2. Synthesis of Gd(cbx-TPT-cbx)1.5 MOF

In a solvothermal approach, the organic linker cbx-TPT-cbx (0.0221 g, 2.78 x10^{-5} mol) was added to a pressure tube and dissolved in DMF (6 mL). An aqueous solution of [$Gd(NO_3)_3$] (5 mL, 1.85 x10-5 mol) was added to the linker solution. The solution was sonicated for 5 minutes, heated at 80 °C for three days, cooled to room temperature for one day, and then stored in a freezer at -29°C for one day. The resulting yellow powder was filtered, washed with acetone, and dried in the air.

3.2.3. MOF activation procedure

The solid was washed three times with 10 mL of ice-cold DMF. The solvent was then exchanged with 10 mL of ice-cold methanol. The MOFs were allowed to soak in methanol overnight before washing three times with 10 mL of ice-cold acetone. After the final wash, the MOFs were thermally activated at 60 °C for 24 hours under reduced pressure.

3.2.4. Single crystal X-ray diffraction

A suitable crystal was mounted on a glass fiber and placed in the low-temperature nitrogen stream of a Bruker SMART CCD area detector diffractometer. A full sphere of data was collected using a graphite-monochromated Mo-Kα radiation source (λ = 0.71073 Å).

3.2.5. Powder X-ray diffraction

Powder X-ray diffraction (PXRD) was performed using a Bruker D2 X-ray diffractometer using Cu Kα radiation (λ= 1.5406 Å). Data were collected over the range of 4˚ < 2(θ) < 60˚ in 0.02˚ steps at a scan rate of 1˚/min. Samples were prepared on a zero-diffraction silicon wafer.

3.2.6. UV-Vis spectra

Absorption spectra were measured on a PerkinElmer Lambda 35 spectrometer equipped with deuterium and tungsten halogen lamps and a concave grating with 1053 lines/mm. The spectra were collected using a scan speed of 480 nm/min in the range 225−600 nm with a photodiode detector. All spectra were background corrected, using solvent as the blank. Spectra of the ligands and standard were collected using concentrations between 0.1-5.0 μM.

3.2.7. Singlet oxygen emission

Singlet oxygen emission was measured on a HORIBA Fluorolog-3 fluorimeter (Horiba FL3-22-iHR550) equipped with using a Hamamatsu 5509−73 NIR detector cooled with liquid N_2 (1 s integration times and 14 nm excitation and emission slit widths were needed).

3.2.8. Determination of singlet oxygen quantum yield

For SOQY experiments, samples were prepared at concentrations where the optical density was below 0.05 and were excited at wavelengths corresponding to that specific optical absorbance (433 nm for cbx-TPT-cbx and 406 nm for 3T). Quantum yields were determined relative to 2,2’:5’,2’’terthiophene (3T) standard, which has a quantum yield of singlet oxygen

production in DCM of 0.75.[33] The SOQY of cbx-2T-cbx, cbx-3T-cbx, and cbx-TPT-cbx were determined by the dilution method using the equation below.

$$\phi_x = \frac{m_x}{m_{\text{std}}} \times \frac{I_{\text{std}}}{I_x} \times \phi_{\text{std}}$$

m is the slope of the plot of the emission area as a function of the absorbance, *I* is the intensity of the excitation source at the excitation wavelength used, and *f* is the quantum yield for sample x, namely cbx-TPT-cbx, and std is the standard, 3T. All data are the average of at least three independent measurements.

3.3. Results and discussion

To investigate new light-activated MOFs for their application in WWT, preliminary studies on the organic linkers and a MOF were performed. The studies conducted were single-crystal X-ray diffraction, powder X-ray diffraction, florescence excitation and emission, UV/Vis absorption, and SOQY. While this preliminary photophysical characterization is incomplete, a foundation has been set for future studies.

3.3.1. Single crystal X-ray diffraction

Cbx-3T-cbx crystallized in the Cc space group with unit cell parameters a = 30.9 Å, b = 17.924 Å, c = 8.0667 Å, V = 4412.30 Å^3, α = 90.0°, β = 99.06 °, and γ = 90.0°. Crystallographic details are summarized and selected information is given in Table 1. The compound structure, shown in Figure 23, consists of three thiophene rings with two 4-aminopyridine-2,6-dicarboxamide functional groups at the 2- and 5’’- positions on the terminal thiophene rings.

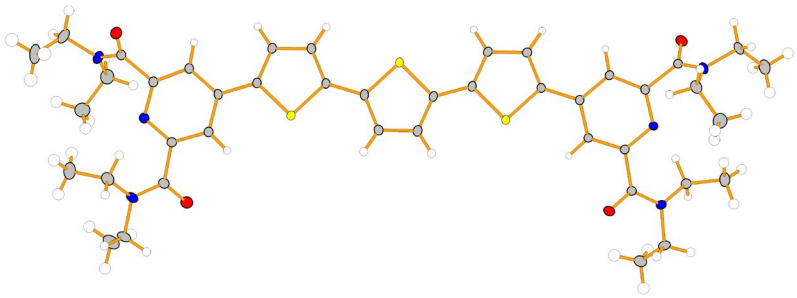

Figure 23. Thermal ellipsoid plot of cbx-3T-cbx. Carbon (grey), nitrogen (blue), oxygen (red), sulfur (yellow), and hydrogen (white).

Identifier	Cbx-3T-cbx
Formula	C_{42} H_{50} N_6 O_5 S_3
Space Group	Cc
Cell Lengths (Å)	**a** 30.9005 **b** 17.9246 **c** 8.0667
Cell Angles (°)	**α** 90.00 **β** 99.06 **γ** 90.00
Cell Volume (Å)	4412.30
R-Factor	7.53

Table 1. Selected crystal structure Information

3.3.2. Powder X-ray diffraction

Typically, analysis of MOFs by PXRD is used as a qualitative technique, by comparing the diffraction patterns of a new material (e.g., MOF) with those of known starting materials (e.g., linkers and metal salts). The PXRD pattern of a Gd(cbx-TPT-cbx)$_{1.5}$ material (red, Figure 24). The powder diffraction peaks are sharp, suggesting a crystalline substance. The green trace shows the simulated PXRD pattern of the organic linker and the black trace shows the pattern of Gd(NO_3)$_3$. The three PXRD patterns are different suggesting that a crystallin material has been synthesized.

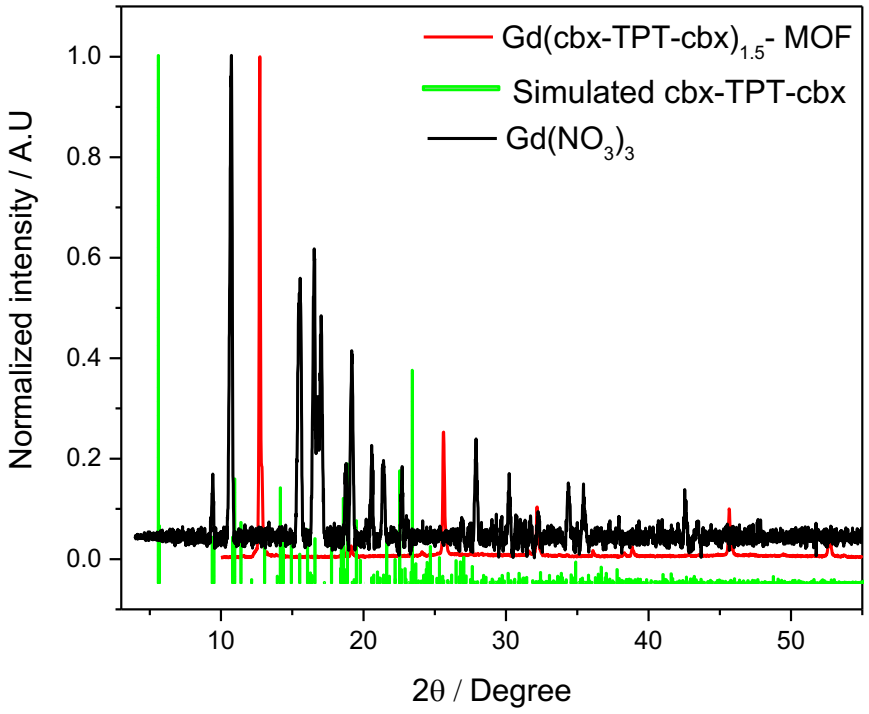

Figure 24. XRD pattern of a Gd(cbx-TPT-cbx)$_{1.5}$ material (Red). Simulated PXRD pattern of cbx-TPT-cbx (Green). PXRD pattern of Gd$(NO_3)_3$ (black).

3.3.3. UV-Vis, excitation, emission, and SO generation of linkers

In acetonitrile, cbx-2T-cbx, cbx-3T-cbx, and cbx-TPT-cbx have absorption maxima at 395, 425, and 405 nm (Figure 25, black) respectively. These compounds emit in the visible region of the spectrum with maxima at 460, 515, and 490 nm (Figure 25, green), respectively. The excitation spectra monitoring ligand emission maxima (Figure 25, blue) show that the absorption and excitation spectra coincide for all compounds. Upon excitation of the three compounds near their absorption maxima (400 nm), SO was generated, as evidenced by its emission at 1270 nm (Figure 26). For cbx-TPT-cbx, cbx-2T-cbx, and cbx-3T-cbx the SOQY are 19. 7 ± 0.9, 37.1 ± 2.3, and 47.4 ± 3.3 %, respectively (Table 2). Figure 27 shows the plots of the SO generation as a function of absorbance of both the cbx-TPT-cbx and the 3T standard in DCM.

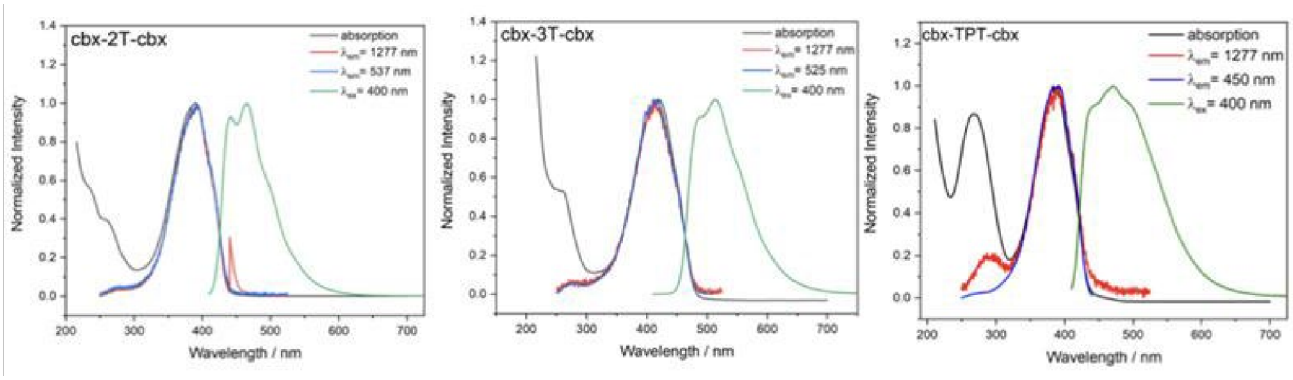

Figures 25. Absorption (black), singlet oxygen excitation (red), compound excitation (blue), and emission (green) spectra of cbx-2T-cbx, cbx-3T-cbx, and cbx-TPT-cbx in acetonitrile. [L]= 1.0 x 10^{-5} M.

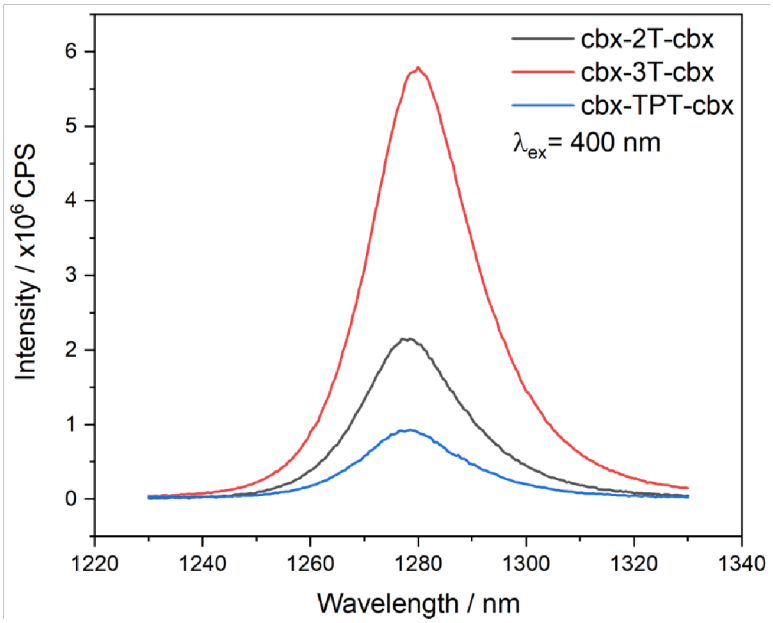

Figure 26. Emission spectra monitoring singlet oxygen phosphorescence the compounds studied here in acetonitrile. [L] = 1.0 × 10^{-5} M.

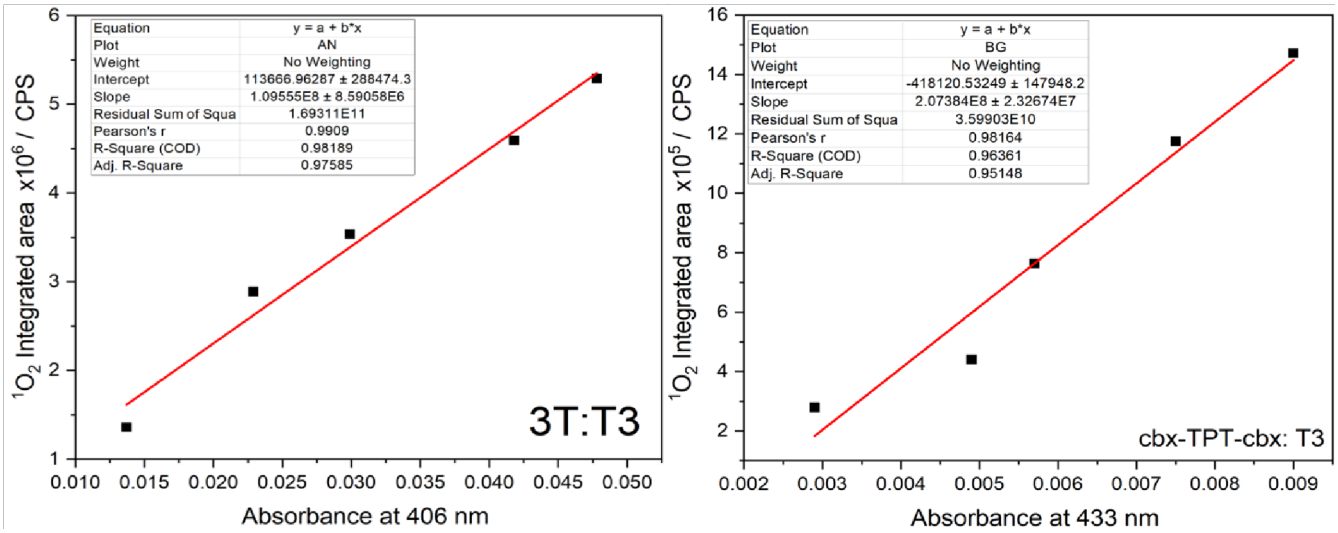

Figure 27. The integrated emission area of singlet oxygen (λ_{ex} = 406 nm) vs. the absorbance monitored at 406 nm for a 3T solution in acetonitrile. [L] = 0.1-0.5 μM (Left graph)
The integrated emission area of singlet oxygen (λ_{ex} = 433 nm) vs the absorbance monitored at 433 nm for a cbx-TPT-cbx solution in acetonitrile. [L] = 1.0-5.0 μM (right graph)

Compound	SOQY (Φ_Δ)
cbx-2T-cbx	37.1 ± 2.3
cbx-3T-cbx	47.4 ± 3.3
cbx-TPT-cbx	19.7 ± 0.9

Table 2. Singlet oxygen quantum yields of the different compounds.

3.4. Summary

Preliminary studies on three ligands and one MOF with potential applications in WWT were performed using various techniques. The crystal structure of cbx-3T-cbx was obtained from SCXRD, and a Gd(cbx-TPT-cbx)$_{1.5}$ material was proven via PXRD to have a crystalline lattice. UV/Vis absorption, ligand excitation, and ligand emission have been shown for cbx-2T-cbx, cbx-3T-cbx, and cbx-TPT-cbx; interestingly, the absorbance maxima for all three compounds is near 400 nm. When comparing the cbx-2T-cbx to the cbx-3T-cbx, a red shift is observed in the

absorbance, consequent of the increase in the conjugation. These compounds SO generation was monitored via phosphoresce emission at 1270 nm, cbx-3T-cbx showed the most vigorous emission, relative to cbx-2T-cbx and cbx-TPT-cbx. The SOQY for cbx-TPT-cbx, cbx-2T-cbx, and cbx-3T-cbx in DCM was shown to be 19.7, 37.1, and 47.4 %, respectively. These compounds have demonstrated their ability to form crystalline compounds, absorb in the visible, and generate SO. The electronic and structural features of these compounds have been exploited for their potential use as photosensitizing adsorbents, that could be implemented into WWT.

4. Chapter 4 – Conclusions

There is a selection of wastewater treatment technologies and materials, which vary in performance and sustainability. Significant factors such as performance, cost, and sustainability are considered to determine the practicality of wastewater technologies. The objective of this study is to introduce new sustainable materials that have promising applications in WWT. Here we have doped PSs, namely 3T, Nap-cbx, and $[Gd(Nap\text{-}cbx)_3](NO_3)_3$ into a polyurethane rubber, forming functional membranes capable of generating SO and which were shown to degrade model pollutants. The membranes' performance and stability were evaluated, and it was shown that the membranes are capable of degrading pollutants after multiple cycles with minimal loss in performance. In addition, preliminary studies on ligands that can be used to construct MOFs were explored. These ligands have demonstrated their ability to absorb in the visible region, generate SO, and coordinate to metals forming extended networks. The design of MOFs that can both adsorb and photo-degrade pollutants is highly desirable for sustainable WWT technologies.

Conflict of Interest

None

References

1 Ferronato, N. & Torretta, V. Waste Mismanagement in Developing Countries: A Review of Global Issues. *Int J Environ Res Public Health* **16**, doi:10.3390/ijerph16061060 (2019).

2 Hashim, N., Yuzir, A., Fadhil Al-Qaim, F. & E.M. Yahaya, N. K. Occurrence and Distribution of 17 Targeted Human Pharmaceuticals in Various Aquatic Environmental Matrices in Southeast Asia with Particular Reference to Malaysia: A Comprehensive Review. *Journal of the Mexican Chemical Society* **65**, doi:10.29356/jmcs.v65i3.1487 (2021).

3 Duque, A. F., Campo, R., Val Del Rio, A. & Amorim, C. L. Wastewater Valorization: Practice around the World at Pilot- and Full-Scale. *Int J Environ Res Public Health* **18**, doi:10.3390/ijerph18189466 (2021).

4 Englande, A. J., Krenkel, P. & Shamas, J. in *Reference Module in Earth Systems and Environmental Sciences* (2015).

5 Hewitt, J., Leonard, M., Greening, G. E. & Lewis, G. D. Influence of wastewater treatment process and the population size on human virus profiles in wastewater. *Water Res* **45**, 6267-6276, doi:10.1016/j.watres.2011.09.029 (2011).

6 Amit Sonune*, R. G. Developments in wastewater treatment methods. *Desalination* **167**, 55-63, doi:10.1016/3.desal.2004.06.113 (2004).

7 B. Je erson*, A. L., S. Parsons, T. Stephenson, S. Judd. Technologies for domestic wastewater recycling. (1999).

8 Watkinson, A. J., Murby, E. J. & Costanzo, S. D. Removal of antibiotics in conventional and advanced wastewater treatment: implications for environmental discharge and wastewater recycling. *Water Res* **41**, 4164-4176, doi:10.1016/j.watres.2007.04.005 (2007).

9 Tran, Q. K., Schwabe, K. A. & Jassby, D. Wastewater Reuse for Agriculture: Development of a Regional Water Reuse Decision-Support Model (RWRM) for Cost-Effective Irrigation Sources. *Environ Sci Technol* **50**, 9390-9399, doi:10.1021/acs.est.6b02073 (2016).

10 How Wastewater treatmeant works… The basics. 6 (1998).

11 Sharma, S. & Bhattacharya, A. Drinking water contamination and treatment techniques. *Applied Water Science* **7**, 1043-1067, doi:10.1007/s13201-016-0455-7 (2016).

12 Bashir, I. *et al.* in *Bioremediation and Biotechnology* Ch. Chapter 1, 1-26 (2020).

13 Peydayesh, M. & Mezzenga, R. Protein nanofibrils for next generation sustainable water purification. *Nat Commun* **12**, 3248, doi:10.1038/s41467-021-23388-2 (2021).

14 HArdy, E. D. Dalecarlia waster treatmeant plant. 9 (1996).

15 de Medeiros, A. D. L. M. *et al.* Biocellulose for Treatment of Wastewaters Generated by Energy Consuming Industries: A Review. *Energies* **14**, doi:10.3390/en14165066 (2021).

16 Tian, X. *et al.* A comprehensive review on toxic petrochemical wastewater pretreatment and advanced treatment. *Journal of Cleaner Production* **245**, doi:10.1016/j.jclepro.2019.118692 (2020).

17 Al Umairi, A. R., How, Z. T. & Gamal El-Din, M. Enhanced primary treatment during wet weather flow using ferrate as a coagulant, coagulant aid and disinfectant. *J Environ Manage* **290**, 112603, doi:10.1016/j.jenvman.2021.112603 (2021).

18 EPA, U. Primer for Municipal Wastewater Treatment Systems. 30 (2004).

19 Wacławek, S. *et al.* Chemistry of persulfates in water and wastewater treatment: A review. *Chemical Engineering Journal* **330**, 44-62, doi:10.1016/j.cej.2017.07.132 (2017).

20 Galal-Gorchev, H. Chlorine in water disinfection. *Pure & Appl. Chem.* **68**, 1731-1735 (1996).

21 Agency, U. S. e. p. Wastewater Tech. Fact sheet chlorine disinfection. (1999).

22 Yang, N. J. & Hinner, M. J. Getting across the cell membrane: an overview for small molecules, peptides, and proteins. *Methods Mol Biol* **1266**, 29-53, doi:10.1007/978-1-4939-2272-7_3 (2015).

23 C. Venkobachar. Leela Iyengar, A. V. S. P. R. Mechanism of disinfection- Effect of chlorine on cell membrane functions. *Water Research* **11**, 727-729 (1976).

24 Kumar, S. *et al.* Total trihalomethanes in public drinking water supply and birth outcomes: a cross-sectional study. *Matern Child Health J* **18**, 996-1006, doi:10.1007/s10995-013-1328-4 (2014).

25 Li, X. F. & Mitch, W. A. Drinking Water Disinfection Byproducts (DBPs) and Human Health Effects: Multidisciplinary Challenges and Opportunities. *Environ Sci Technol* **52**, 1681-1689, doi:10.1021/acs.est.7b05440 (2018).

26 Han, J., Zhang, X., Jiang, J. & Li, W. How Much of the Total Organic Halogen and Developmental Toxicity of Chlorinated Drinking Water Might Be Attributed to Aromatic Halogenated DBPs? *Environ Sci Technol* **55**, 5906-5916, doi:10.1021/acs.est.0c08565 (2021).

27 Al-Abri, M. *et al.* Chlorination disadvantages and alternative routes for biofouling control in reverse osmosis desalination. *npj Clean Water* **2**, doi:10.1038/s41545-018-0024-8 (2019).

28 Richardson, S. Disinfection by-products and other emerging contaminants in drinking water. *TrAC Trends in Analytical Chemistry* **22**, 666-684, doi:10.1016/s0165-9936(03)01003-3 (2003).

29 Collivignarelli, M., Abbà, A., Benigna, I., Sorlini, S. & Torretta, V. Overview of the Main Disinfection Processes for Wastewater and Drinking Water Treatment Plants. *Sustainability* **10**, doi:10.3390/su10010086 (2017).

30 Ao, X. W. *et al.* Peracetic acid-based advanced oxidation processes for decontamination and disinfection of water: A review. *Water Res* **188**, 116479, doi:10.1016/j.watres.2020.116479 (2021).

31 Xu, M. *et al.* MOF laminates functionalized polyamide self-cleaning membrane for advanced loose nanofiltration. *Separation and Purification Technology* **275**, doi:10.1016/j.seppur.2021.119150 (2021).

32 Ogilby, P. R. Singlet oxygen: there is indeed something new under the sun. *Chem Soc Rev* **39**, 3181-3209, doi:10.1039/b926014p (2010).

33 Becker, R. S. Comprehensive Evaluation of the Absorption, Photophysical, Energy Transfer, Structural, and Theoretical Properties of r-Oligothiophenes with One to Seven Rings. *J. Phys. Chem*, 18683-18695 (1996).

34 Moosavi, S. M. *et al.* Capturing chemical intuition in synthesis of metal-organic frameworks. *Nat Commun* **10**, 539, doi:10.1038/s41467-019-08483-9 (2019).

35 Safdar, M., Ghazy, A., Lastusaari, M. & Karppinen, M. Lanthanide-based inorganic–organic hybrid materials for photon-upconversion. *Journal of Materials Chemistry C* **8**, 6946-6965, doi:10.1039/d0tc01216e (2020).

36 Zhang, J., Wu, S., Lu, X., Wu, P. & Liu, J. Lanthanide-Boosted Singlet Oxygen from Diverse Photosensitizers along with Potent Photocatalytic Oxidation. *ACS Nano* **13**, 14152-14161, doi:10.1021/acsnano.9b06840 (2019).

37 Macia, N., Bresoli-Obach, R., Nonell, S. & Heyne, B. Hybrid Silver Nanocubes for Improved Plasmon-Enhanced Singlet Oxygen Production and Inactivation of Bacteria. *J Am Chem Soc* **141**, 684-692, doi:10.1021/jacs.8b12206 (2019).

38 Wasserman, H. H. SINGLET OXYGEN IN ORGANIC SYNTHESIS. *Tetrahedron* **37** (1980).

39 M. Orfanopoulos, I. S., and Christopher S. Foote. Intermediates in the ene reactions of singlet oxygen and N-phenyl-1,2,4-triazoline-3,5-dione with olefins. *J. Am. Chem. Soc.* **112** (1990).

40 Foote*, P. K. a. C. S. Formation of Transient Intermediates in Low-Temperature Photosensitized Oxidation of an 8-13C-Guanosine Derivative. *JACS* **124** (2002).

41 Garcia-Calvo, J. *et al.* Fluorescent Membrane Tension Probes for Super-Resolution Microscopy: Combining Mechanosensitive Cascade Switching with Dynamic-Covalent Ketone Chemistry. *J Am Chem Soc* **142**, 12034-12038, doi:10.1021/jacs.0c04942 (2020).

42 García-Fresnadillo, D. Singlet Oxygen Photosensitizing Materials for Point-of-Use Water Disinfection with Solar Reactors. *ChemPhotoChem* **2**, 512-534, doi:10.1002/cptc.201800062 (2018).

43 Markovic, Z. M. *et al.* Antibacterial photodynamic activity of carbon quantum dots/polydimethylsiloxane nanocomposites against Staphylococcus aureus, Escherichia coli and Klebsiella pneumoniae. *Photodiagnosis Photodyn Ther* **26**, 342-349, doi:10.1016/j.pdpdt.2019.04.019 (2019).

44 Khalid, A. *et al.* Bismuth sulfide photocatalysis water treatment under visible irradiation. *Research on Chemical Intermediates* **47**, 3395-3409, doi:10.1007/s11164-021-04471-1 (2021).

45 Tortajada, C. Contributions of recycled wastewater to clean water and sanitation Sustainable Development Goals. *npj Clean Water* **3**, doi:10.1038/s41545-020-0069-3 (2020).

46 Wu, J., Cao, M., Tong, D., Finkelstein, Z. & Hoek, E. M. V. A critical review of point-of-use drinking water treatment in the United States. *npj Clean Water* **4**, doi:10.1038/s41545-021-00128-z (2021).

47 Su, L. *et al.* Chitosan-riboflavin composite film based on photodynamic inactivation technology for antibacterial food packaging. *Int J Biol Macromol* **172**, 231-240, doi:10.1016/j.ijbiomac.2021.01.056 (2021).

48 Kadhom, M. & Deng, B. Metal-organic frameworks (MOFs) in water filtration membranes for desalination and other applications. *Applied Materials Today* **11**, 219-230, doi:10.1016/j.apmt.2018.02.008 (2018).

49 Huang, W. *et al.* A natural impact-resistant bicontinuous composite nanoparticle coating. *Nat Mater* **19**, 1236-1243, doi:10.1038/s41563-020-0768-7 (2020).

50 Sortino, S., Petralia, S., Bosca, F. & Miranda, M. A. Irreversible photo-oxidation of propranolol triggered by self-photogenerated singlet molecular oxygen. *Photochem Photobiol Sci* **1**, 136-140, doi:10.1039/b109232d (2002).

51 Xiong, R. *et al.* UV-LED/chlorine degradation of propranolol in water: Degradation pathway and product toxicity. *Chemosphere* **248**, 125957, doi:10.1016/j.chemosphere.2020.125957 (2020).

52 Becker-Jahn, J. *et al.* Photoactive polymer membranes for degradation of pharmaceuticals from water. *Catalysis Today* **364**, 256-262, doi:10.1016/j.cattod.2020.05.017 (2021).

53 Johnson, K. R. & de Bettencourt-Dias, A. (1)O2 Generating Luminescent Lanthanide Complexes with 1,8-Naphthalimide-Based Sensitizers. *Inorg Chem* **58**, 13471-13480, doi:10.1021/acs.inorgchem.9b02431 (2019).

54 Khurram, R., Wang, Z. & Ehsan, M. F. alpha-Fe2O3-based nanocomposites: synthesis, characterization, and photocatalytic response towards wastewater treatment. *Environ Sci Pollut Res Int* **28**, 17697-17711, doi:10.1007/s11356-020-11778-w (2021).

55 Patel, M. *et al.* Pharmaceuticals of Emerging Concern in Aquatic Systems: Chemistry, Occurrence, Effects, and Removal Methods. *Chem Rev* **119**, 3510-3673, doi:10.1021/acs.chemrev.8b00299 (2019).

56 Lu, S., Liu, L., Demissie, H., An, G. & Wang, D. Design and application of metal-organic frameworks and derivatives as heterogeneous Fenton-like catalysts for organic wastewater treatment: A review. *Environ Int* **146**, 106273, doi:10.1016/j.envint.2020.106273 (2021).

57 Hou, J. *et al.* Metal-organic framework crystal-glass composites. *Nat Commun* **10**, 2580, doi:10.1038/s41467-019-10470-z (2019).

58 Babaei, H. *et al.* Observation of reduced thermal conductivity in a metal-organic framework due to the presence of adsorbates. *Nat Commun* **11**, 4010, doi:10.1038/s41467-020-17822-0 (2020).

59 James, S. L. Metal-organic frameworks. *Chem Soc Rev* **32**, 276-288, doi:10.1039/b200393g (2003).

60 Li, J., Wang, H., Yuan, X., Zhang, J. & Chew, J. W. Metal-organic framework membranes for wastewater treatment and water regeneration. *Coordination Chemistry Reviews* **404**, doi:10.1016/j.ccr.2019.213116 (2020).

61 Farha, O. K. *et al.* Metal-organic framework materials with ultrahigh surface areas: is the sky the limit? *J Am Chem Soc* **134**, 15016-15021, doi:10.1021/ja3055639 (2012).

62 Zhang, D. *et al.* MOFs-derived magnetic C@Cu-Ni bimetal particles: An efficient peroxymonosulfate activator for 2,4,6-trichlorophenol degradation. *Chemosphere* **269**, 129394, doi:10.1016/j.chemosphere.2020.129394 (2021).

63 Sun, T., Gao, Y., Du, Y., Zhou, L. & Chen, X. Recent Advances in Developing Lanthanide Metal-Organic Frameworks for Ratiometric Fluorescent Sensing. *Front Chem* **8**, 624592, doi:10.3389/fchem.2020.624592 (2020).

64 Mishra, Y. K. *et al.* Removal of organic contaminants from wastewater with GO/MOFs composites. *Plos One* **16**, doi:10.1371/journal.pone.0253500 (2021).

65 Li, Z. *et al.* Note: Measuring instrument of singlet oxygen quantum yield in photodynamic effects. *Rev Sci Instrum* **88**, 066102, doi:10.1063/1.4985111 (2017).

66 Xia, X. *et al.* A Review Study on Sulfate-Radical-Based Advanced Oxidation Processes for Domestic/Industrial Wastewater Treatment: Degradation, Efficiency, and Mechanism. *Front Chem* **8**, 592056, doi:10.3389/fchem.2020.592056 (2020).

67 Buru, C. T. *et al.* Improving the Efficiency of Mustard Gas Simulant Detoxification by Tuning the Singlet Oxygen Quantum Yield in Metal-Organic Frameworks and Their Corresponding Thin Films. *ACS Appl Mater Interfaces* **10**, 23802-23806, doi:10.1021/acsami.8b05792 (2018).

68 Wu, Z. *et al.* Aromatic heterocycle-grafted NH2-MIL-125(Ti) via conjugated linker with enhanced photocatalytic activity for selective oxidation of alcohols under visible light. *Applied Catalysis B: Environmental* **224**, 479-487, doi:10.1016/j.apcatb.2017.10.034 (2018).

69 Wang, P. *et al.* A broadband and strong visible-light-absorbing photosensitizer boosts hydrogen evolution. *Nat Commun* **10**, 3155, doi:10.1038/s41467-019-11099-8 (2019).

70 Zhao, J. *et al.* Transition metal complexes with strong absorption of visible light and long-lived triplet excited states: from molecular design to applications. *RSC Adv.* **2**, 1712-1728, doi:10.1039/c1ra00665g (2012).

71 Russo, V. *et al.* Applications of Metal Organic Frameworks in Wastewater Treatment: A Review on Adsorption and Photodegradation. *Frontiers in Chemical Engineering* **2**, doi:10.3389/fceng.2020.581487 (2020).

72 Seetharaj, R., Vandana, P. V., Arya, P. & Mathew, S. Dependence of solvents, pH, molar ratio and temperature in tuning metal organic framework architecture. *Arabian Journal of Chemistry* **12**, 295-315, doi:10.1016/j.arabjc.2016.01.003 (2019).